Oxytocin selectively excites interneurons and inhibits output neurons of the bed nucleus of the stria terminalis (BNST)

Running title: Oxytocin regulates intrinsic inhibitory network of the BNST

Walter Francesconi [1,2], Fulvia Berton [1,2], Valentina Olivera-Pasilio [1,2,3], and Joanna Dabrowska [1,2,3]

[1] Center for the Neurobiology of Stress Resilience and Psychiatric Disorders, Rosalind Franklin University of Medicine and Science, North Chicago, IL 60064, USA

[2] Discipline of Cellular and Molecular Pharmacology, Chicago Medical School, Rosalind Franklin University of Medicine and Science, North Chicago, IL 60064, USA

[3] School of Graduate and Postdoctoral Studies, Rosalind Franklin University of Medicine and Science, North Chicago, IL 60064, USA

* To whom correspondence should be addressed:

Joanna Dabrowska, Center for the Neurobiology of Stress Resilience and Psychiatric Disorders, Rosalind Franklin University of Medicine and Science, North Chicago, IL 60064, USA

joanna.dabrowska@rosalindfranklin.edu

Phone: (847) 578-8664

Fax: (847) 578-3268

Number of figures (7), number of tables (1)

Abstract

The dorsolateral bed nucleus of the stria terminalis ($BNST_{DL}$) has high expression of oxytocin receptors, but their role in the modulation of $BNST_{DL}$ activity remains elusive. $BNST_{DL}$ contains GABA-ergic neurons classified based on intrinsic membrane properties into three types. Using *in vitro* patch-clamp and cell-attached recordings in male rats, we demonstrate that oxytocin excites and increases spontaneous firing of Type I, putative $BNST_{DL}$ interneurons. As a consequence, oxytocin increases the frequency of spontaneous inhibitory post-synaptic currents (sIPSCs) (tetrodotoxin-sensitive) and reduces spontaneous firing of Type II neurons. In contrast, in Type III neurons, oxytocin reduces the amplitude of both sIPSCs and evoked IPSCs, suggesting a direct postsynaptic inhibitory effect. As Type II and Type III are the $BNST_{DL}$ projection neurons, we present a model of fine-tuned modulation by oxytocin, which selectively excites Type I $BNST_{DL}$ interneurons and inhibits Type II and Type III output neurons, via an indirect and direct mechanism, respectively.

48 ***1. Introduction***

49 Oxytocin (OT) is a nine amino acid peptide serving as a hypothalamic hormone, which regulates
50 uterine contractions during labor, milk ejection reflex during lactation (Caldeyro-Barcia and
51 Poseiro, 1959; Nickerson et al., 1954), as well as water-electrolyte balance (Han et al., 1993;
52 Verbalis et al., 1993). As a neuromodulator in the central nervous system, OT facilitates social
53 behaviors (Bosch and Young, 2018; Pedersen et al., 1992; Tabbaa et al., 2016), regulates
54 stress response, stress-coping behaviors, and fear and anxiety-like behaviors, for review see
55 (Janeček and Dabrowska, 2019; Neumann and Slattery, 2016; Olivera-Pasilio and Dabrowska,
56 2020). Although OT has been shown to modulate fear responses primarily in the central
57 amygdala (CeA) (Knobloch et al., 2012; Terburg et al., 2018; Viviani et al., 2011), we recently
58 showed that oxytocin receptor (OTR) transmission in the dorsolateral bed nucleus of the stria
59 terminalis ($BNST_{DL}$) facilitates the formation of cued fear and improves fear discrimination to
60 signaled vs. un-signaled threats (Martinon et al., 2019; Moaddab and Dabrowska, 2017), for
61 review see (Olivera-Pasilio and Dabrowska, 2020).

62 On a cellular level, OT has shown robust modulatory influence on the neurocircuitry of
63 the hippocampus (Harden and Frazier, 2016; Maniezzi et al., 2019; Owen et al., 2013; Tirko et
64 al., 2018), auditory cortex (Marlin et al., 2015), ventral tegmental area, VTA, (Hung et al., 2017;
65 Xiao et al., 2017), and the CeA (Huber et al., 2005; Knobloch et al., 2012; Terburg et al., 2018;
66 Viviani et al., 2011). Notably, although the BNST has one of the highest expression levels of
67 OTR in the rodent brain (Dabrowska et al., 2011; Dumais et al., 2013; Tribollet et al., 1992;
68 Veinante and Freund-Mercier, 1997) and receives OT inputs from hypothalamic nuclei
69 (Dabrowska et al., 2011; Knobloch et al., 2012; Martinon et al., 2019), the effects of OT on
70 excitability and synaptic transmission of BNST neurons remain unknown. Studies in the 90's
71 from the Ingram group using electrophysiological approaches have shown that OT increases the
72 spontaneous firing frequency in a subpopulation of BNST neurons in lactating female rats

73 (Ingram et al., 1990; Ingram and Moos, 1992; Wilson et al., 2005), but their phenotype is not
74 known.

75 $BNST_{DL}$ neurons are GABA-ergic (Cullinan et al., 1993; Dabrowska et al., 2013a; Sun
76 and Cassell, 1993), and functionally interconnected via a dense intrinsic inhibitory network (Xu
77 et al., 2016). As originally described by Rainnie and colleagues, $BNST_{DL}$ neurons can be
78 classified into three major neuron types (I-III) based on their electrophysiological phenotype
79 defined as a unique pattern of voltage deflection in response to transient depolarizing and
80 hyperpolarizing current injections (Daniel et al., 2017; Hammack et al., 2007) and/or based on a
81 single-cell mRNA expression of ion channel subunits (Hazra et al., 2011). Recently, it was
82 shown that both Type II and Type III are output neurons of the $BNST_{DL}$, with major projections to
83 the CeA (mainly Type II neurons), lateral hypothalamus (LH), and the VTA (mainly Type III
84 neurons) (Yamauchi et al., 2018).

85 In the current study, using *in vitro* slice patch-clamp recordings in a whole-cell and cell-
86 attached mode, we investigated the effects of OT on intrinsic excitability, inhibitory synaptic
87 transmission and spontaneous firing in Type I-III $BNST_{DL}$ neurons in male Sprague-Dawley rats.
88 We show that OT is a powerful modulator of the intrinsic inhibitory network such as it selectively
89 increases the intrinsic excitability and the frequency of spontaneous firing of regular spiking,
90 Type I neurons, which leads to increased inhibitory synaptic transmission (spontaneous
91 Inhibitory Postsynaptic Currents, sIPSCs) and reduced spontaneous firing rate of Type II
92 $BNST_{DL}$ neurons. We also combined injections of a fluorescent retrograde tracer into the CeA
93 with electrophysiological recordings from fluorescent $BNST_{DL}$ neurons and we confirm that all
94 recorded CeA-projecting (*BNST➔CeA*) neurons are Type II neurons. Finally, we demonstrate
95 that OT reduces the amplitude of both spontaneous and evoked IPSCs selectively in Type III
96 neurons via a direct, OTR-dependent, postsynaptic mechanism. These results show that OT
97 directly excites Type I $BNST_{DL}$ interneurons and inhibits two classes of the $BNST_{DL}$ output
98 neurons via an indirect (Type II neurons) and a direct (Type III neurons) mechanism.

2. Results

2.1. The effects of OT on intrinsic membrane properties and spontaneous firing in Type I-III $BNST_{DL}$ neurons.

Whole-cell patch-clamp recordings were performed from $BNST_{DL}$ neurons, primarily in the oval nucleus of the BNST ($BNST_{OV}$). At the beginning of the recording sessions in current clamp mode, neurons were electrophysiologically characterized into three types (Type I-III) using current pulses (450 msec in duration) from -350 pA to 80 pA in 5 or 10 pA increments. Based on their characteristic voltage responses (Hammack et al., 2007), three types of neurons were identified in the $BNST_{DL}$ (see Methods for details). We investigated the effects of OT (0.2 μM based on (Crane et al., 2020; Xiao et al., 2017) on intrinsic membrane properties: resting membrane potential (RMP), input resistance (Rin), rheobase (Rh), threshold of the first action potential (Th) (calculated as the voltage at which the depolarization rate exceeded 5 mV/ms), and latency of the first spike (Lat) evoked at the Rh current. Intrinsic membrane properties were investigated in a presence of synaptic transmission's blockers. In Type I neurons, OT induced a significant depolarization of RMP from -62.39 ± 0.84 mV to -57.94 ± 1.39 mV in comparison to baseline (pre, P = 0.0013) and washout (post, P = 0.0304, **Fig. 1A-B**). This was associated with a significant increase of Rin from 170.98 ± 8.6 MΩ to 233.64 ± 18.6 MΩ (P = 0.0085, **Fig. 1C**). As a consequence, OT induced a significant reduction of Rh from 21.96 ± 2.29 pA to 17.32 ± 2.26 pA (P = 0.0023, **Fig. 1D**). The Th of the first spike was also significantly reduced from -38.38 ± 0.68 mV to -39.75 ± 0.88 mV after OT (P = 0.0346**, Fig. 1E**). When the selective and potent OTR antagonist, d(CH2)5(1), D-Tyr(2), Thr(4), Orn(8), des-Gly-NH2(9)]-Vasotocin trifluoroacetate salt (Manning et al., 2012) (0.4 μM, OTA) was applied for 10 min before and during OT application, OT did not significantly affect RMP (P = 0.0710), Rh (P = 0.1231), Th (P = 0.3532) or Lat (P = 0.6252, **not shown**). In contrast to Type I neurons, OT did not affect the intrinsic membrane properties of Type II and III neurons (**Table 1**).

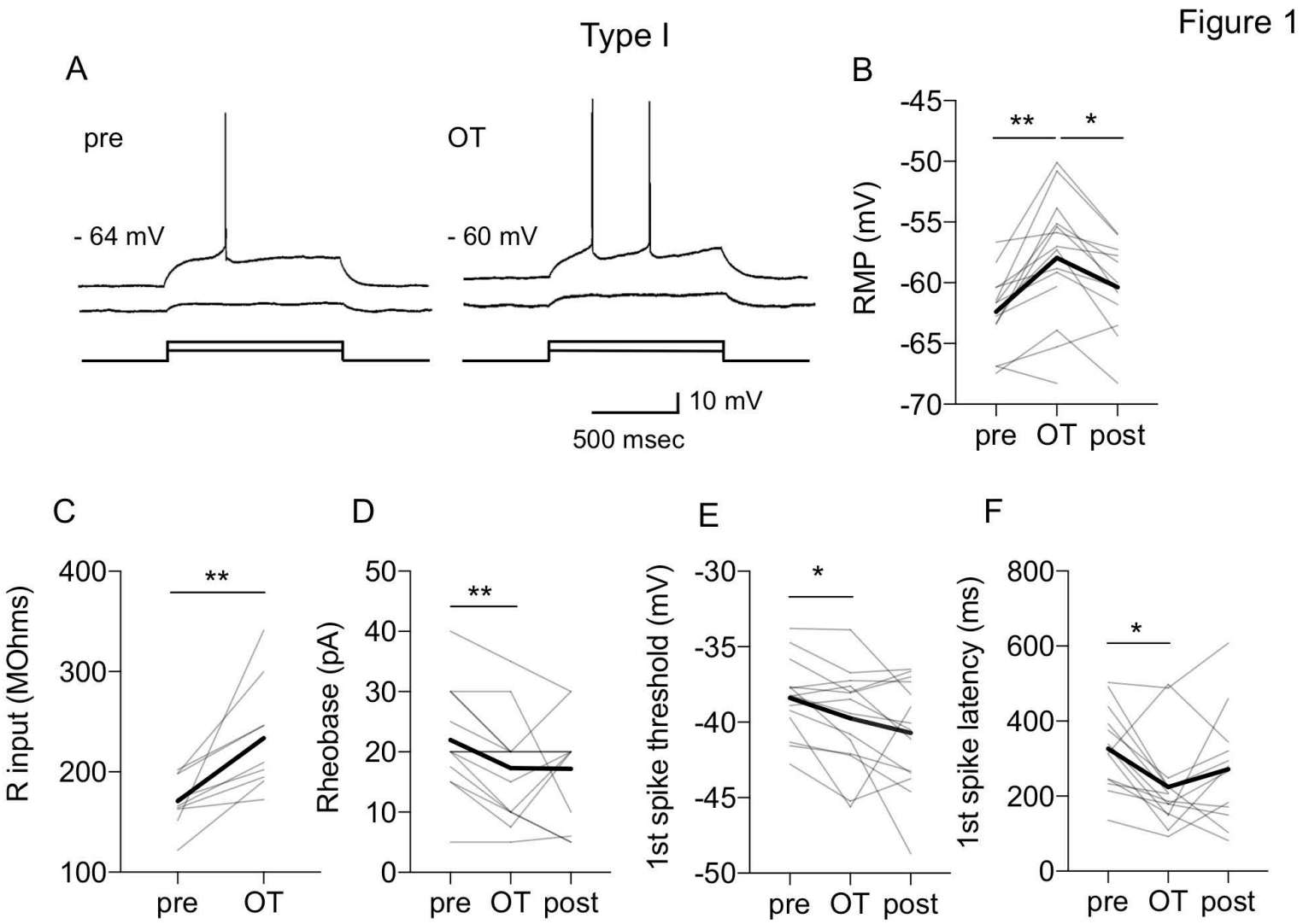

Figure 1. **Oxytocin affects intrinsic membrane properties of Type I $BNST_{DL}$ neurons. A**: A representative trace showing that oxytocin (OT, 0.2 μM) shortens the latency to the 1st spike at rheobase current (Rh) and depolarizes resting membrane potential (RMP, from -64 mV to -60 mV). This is associated with increased input resistance (Rin), measured with a depolarizing current step below the Rh. OT also reduces Rh from 30 pA (pre) to 20 pA (OT) **B-D**: Line graphs with individual neurons' responses (thin gray) and average responses for all neurons recorded (thick black) showing that OT significantly increases the RMP (**B**, $P = 0.0002$, F (1.593, 19.12) = 15.76, n = 14, mixed-effect analysis), increases Rin (**C**, $P = 0.0085$, n = 9, paired t-test), reduces the Rh (**D**, $P = 0.0457$, F (1.341, 16.09) = 4.226, n = 14, mixed-effect analysis), reduces the 1st spike threshold (**E**, P = 0.0164, F (1.472, 20.61) = 5.749, and reduced the 1st spike latency (**F**, $P = 0.0185$, F (1.971, 23.66) = 4.775, n = 14, mixed-effect analysis). Thick black lines show average responses for all Type I neurons recorded, **$P < 0.01$, *$P < 0.05$ in comparison to pre or post-OT.

Table 1. Intrinsic membrane properties and firing activity of Type I-III $BNST_{DL}$ neurons after OT (0.2 μM) application respective to baseline (pre-OT). ****$P < 0.0001$, **$P < 0.01$, *$P < 0.05$. In Type II neurons OT did not affect RMP ($P = 0.0985$), Rin ($P = 0.1377$), Rh ($P = 0.0964$), or Th ($P = 0.5027$). Similarly, in Type III neurons OT did not significantly change RMP ($P = 0.1066$), Rin ($P = 0.0788$), Rh ($P = 0.1664$), or Th ($P = 0.5150$).

Type I neurons	**Pre**	**OT**
RMP (mV)	-62.39 ± 0.84	**57.94 ± 1.39 ****
Rin (MOhms)	170.98 ± 8.6	**233.64 ± 18.6 ***
Rh (pA)	21.96 ± 2.29	**17.32 ± 2.26 ****
Th (mV)	-38.38 ± 0.68	**39.75 ± 0.88 ***
Lat (ms)	326.44 ± 28.63	**224.58 ± 32.51 ****
fAHP (mV)	8.63 ± 0.89	**7.47 ± 0.77 ****
mAHP (mV)	10.69 ± 0.61	**8.45 ± 0.72 ******
lAHP (mV)	0.49 ± 0.12	0.41 ± 0.1
Type II neurons		
RMP (mV)	-57.04 ± 0.86	-56.74 ± 0.78
Rin (MOhms)	221.8 ± 29.27	276.03 ± 46.66
Rh (pA)	16.92 ± 2.52	15 ± 2.66
Th (mV)	-39.87 ± 0.95	-40.32 ± 1.05
Type III neurons		
RMP (mV)	-65.73 ± 1.42	-63.3 ± 1.83
Rin (MOhms)	120.66 ± 23.12	156.93 ± 29.7
Rh (pA)	56.46 ± 8.92	48.33 ± 7.36
Th (mV)	-37.28 ± 0.85	-37.08 ± 0.93

124 We also investigated spiking ability by measuring the input-output (I-O) relationship
125 before and after OT application. The steady state frequency (SSF) was measured by applying
126 depolarizing pulses (1 sec in duration) of different amplitudes (0-80 pA in 10 pA increments).
127 The SSF was determined as the average of the inverse of the inter-spike intervals (ISI) from all
128 action potentials starting from the second action potential. The I/O curve was built before (pre),
129 during, and after OT application (post). OT caused a leftward shift of input/output (I-O)
130 relationship in Type I neurons, demonstrating a significant increment effect on SSF at 40 pA, 50
131 pA, and 60 pA. Post-hoc test showed a significant increase of the SSF after OT from 6.81 ±
132 0.68 Hz to 8.96 ± 0.63 Hz in comparison to baseline (pre, P = 0.0032) and washout (post, P =
133 0.0095) at 40 pA; from 8.73 ± 0.73 Hz to 11.20 ± 0.70 Hz (P = 0.0163, pre and P = 0.0226, post)
134 at 50 pA; and from 9.22 ± 0.57 Hz to 11.89 ± 0.99 Hz (P = 0.0271, pre and P = 0.0054, post) at
135 60 pA. The OT effect reached a trend at 30 pA (from 5.64 ± 0.5 Hz to 7.31 ± 0.53 Hz, P =
136 0.0820) and at 70 pA (from 10.79 ± 0.6 Hz to 13.62 ± 0.99 Hz, P = 0.0794). The effect was not
137 significant at 20 pA (P = 0.1268) and 80 pA (P = 0.1320, **Fig. 2A-B**). Importantly, in the
138 presence of OTA, OT did not affect the SSF of Type I neurons at 80 pA (P = 0.7960), 70 pA (P
139 = 0.4237), 60 pA (P = 0.6312), 50 pA (P = 0.4299), 40 pA (P = 0.3365), or 30 pA (P = 0.4817,
140 **Fig. 2C**). OT did not affect SSF in Type II and Type III neurons (**Fig. 2D-E**).

141 This increase in the spiking ability of Type I neurons after OT was associated with a
142 significant shortening of the first spike's latency from 326.44 ± 28.63 msec to 224.58 ± 32.51
143 msec (P = 0.0083, **Fig. 1F**).

144 A variety of afterhyperpolarizations (AHPs) following a single or a train of action
145 potentials have been described to regulate the neuron excitability and spike frequency
146 adaptation (Gu et al., 2008; Lopez de Armentia and Sah, 2004). They come in a temporal
147 sequence of three AHPs: the fast AHP (fAHP) lasting 1-5 msec, the medium AHP (mAHP)
148 lasting 50-200 msec, which is responsible for early spike frequency adaptation during a train of
149 action potentials, and the late AHP (lAHP) lasting several seconds after a train of action
150 potentials (Gu et al., 2005a). We investigated the effect of the OT on the amplitude of fAHP,

Figure 2

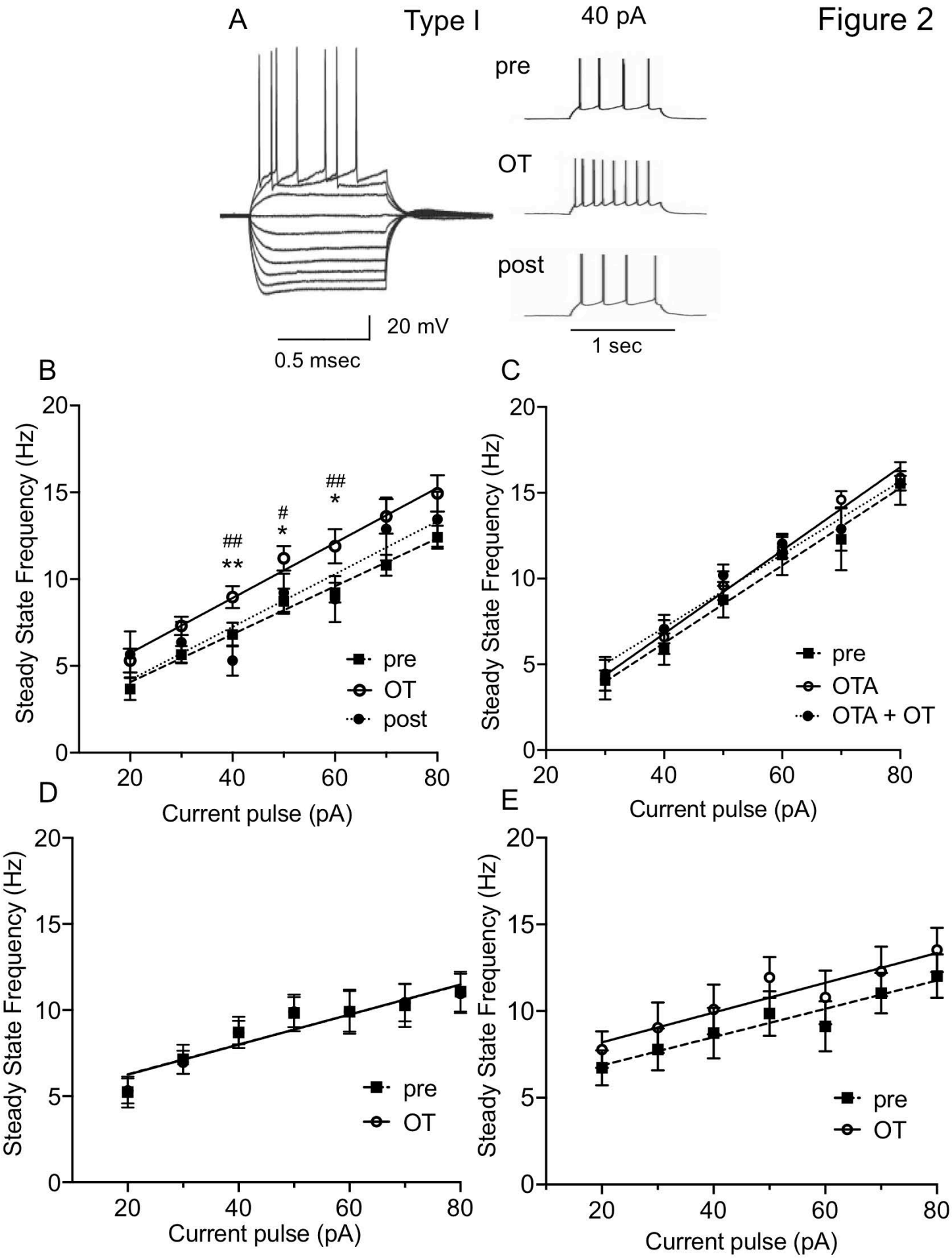
A
Type I
40 pA
pre
OT
post
20 mV
0.5 msec
1 sec
B
Steady State Frequency (Hz)
Current pulse (pA)
##
**
#
*
##
*
pre
OT
post
C
Steady State Frequency (Hz)
Current pulse (pA)
pre
OTA
OTA + OT
D
Steady State Frequency (Hz)
Current pulse (pA)
pre
OT
E
Steady State Frequency (Hz)
Current pulse (pA)
pre
OT

Figure 2. **Oxytocin increases intrinsic excitability of Type I, but not Type II or Type III, $BNST_{DL}$ neurons**. **A**: A representative trace showing voltage deflections in response to hyperpolarizing and depolarizing current injections characteristic of Type I neuron (left) and the increase in firing frequency of Type I neuron in the presence of OT respective to baseline (pre) (right). **B**: OT causes a leftward shift of input/output (I-O) relationship in Type I neurons. The steady state frequency (SSF) was determined as an average of an inverse of the inter-spike intervals (ISI) from all action potentials starting from the second action potential. In Type I neurons, OT shows a significant increment effect on SSF at 40 pA (P = 0.0024, F (1.667, 15.01) = 10.11), at 50 pA (P = 0.0271, F (1.863, 16.76) = 4.628), and at 60 pA (P = 0.0271, F (1.688, 11.82) = 5.267, mixed-effects analysis). **C**: Application of OTR antagonist, OTA (0.4 μM), prevents the leftward shift of the I-O relationship induced by OT application (40 pA, P = 0.3365, 50 pA, P = 0.4299, 60 pA, P = 0.6312, n = 5, RM ANOVA). **D-E**: OT application does not modify the I-O relationship in Type II (**D**) or Type III $BNST_{DL}$ neurons (**E**). In Type II neurons, OT did not affect SSF at 80 pA (P = 0.3116), 70 pA (P = 0.8236), 60 pA (P = 0.9519), 50 pA (P = 0.8993), 40 pA (P = 0.7636), 30 pA (P = 0.8673), or at 20 pA (P = 0.6990, **D**). Similarly, in Type III neurons, there was no effect of OT on SSF at 80 pA (P = 0.1151), 70 pA (P = 0.1138), 60 pA (P = 0.180), 50 pA (P = 0.0847), 40 pA (P = 0.1041), 30 pA (P = 0.0790), or at 20 pA (P = 0.0681, **E**). Each data point represents the mean ± SEM, **P < 0.01, *P < 0.05 in comparison to pre-OT, ## P < 0.01, # P < 0.05 in comparison to post-OT.

151 mAHP and lAHP in all types of the $BNST_{DL}$ neurons and show that OT significantly reduced the
152 amplitude of fAHP (from 8.63 ± 0.89 mV to 7.47 ± 0.77 mV, *P* = 0.0062, **Fig. 3A-B**) and mAHP
153 (from 10.69 ± 0.61 mV to 8.45 ± 0.72 mV, *P* = 0.0001 vs. pre, and *P* = 0.0003 vs. post), **Fig. 3A,**
154 **D**). Notably, OT did not affect the amplitudes of fAHP (*P* = 0.2220, **Fig. 3C**) and mAHP (*P* =
155 0.3968, **Fig. 3E**) in the presence of OTA. Lastly, OT did not significantly affect the amplitude of
156 lAHP (*P* = 0.2401, **not shown**).

157 We also investigated if these changes in AHP amplitude could modify the spike
158 frequency adaptation. We measured the instantaneous frequency for every action potential
159 interval. The ISI number is the inter-stimulus interval between two consecutive action potentials.
160 We found that OT significantly increased the instantaneous frequency of ISIs and post-hoc test
161 showed a significant OT effect on frequency (in Hz) of ISI number 2 (ISI-2) from 16.77 ± 1.55 to
162 19.57 ± 1.2 (*P* = 0.0006), ISI-3 from 12.48 ± 0.88 to 16.19 ± 1.09 (*P* < 0.0001), ISI-4 from 11.92
163 ± 0.88 to 14.87 ± 0.76 (*P* = 0.0006), ISI-5 from 11.36 ± 0.68 to 14.58 ± 0.77 (*P* = 0.0001), ISI-6
164 from 11.26 ± 0.72 to 13.93 ± 0.76 (*P* = 0.0079), and ISI-7 from 10.58 ± 0.64 o 13.44 ± 0.88 (*P* =
165 0.0051, **Fig. 3F**).

166 The spontaneous firing activity of Type I and II $BNST_{DL}$ neurons was recorded in a cell-
167 attached voltage-clamp mode without synaptic transmission's blockers. During cell-attached
168 recordings, the spontaneous firing was present in 7 out of 9 Type I neurons and OT significantly
169 increased the firing rate in the spontaneously firing neurons from 0.88 ± 0.66 Hz to 2.19 ± 0.93
170 Hz (*P* = 0.0242, paired *t*-test, **Fig. 4A-B**). In addition, although only 6 out of 18 Type II neurons
171 showed spontaneous firing in a cell-attached mode, in all spontaneously firing Type II neurons,
172 OT reduced the firing rate from 1.85 ± 0.74 Hz to 1.15 ± 0.69 Hz, which nearly reached
173 statistical significance (*P* = 0.0525, paired *t*-test, **Fig. 4C-D**).

174 Overall, these results suggest that OT increases the intrinsic excitability and facilitates
175 the spontaneous firing selectively in Type I $BNST_{DL}$ neurons, whereas it reduces spontaneous
176 firing rate in Type II $BNST_{DL}$ neurons.

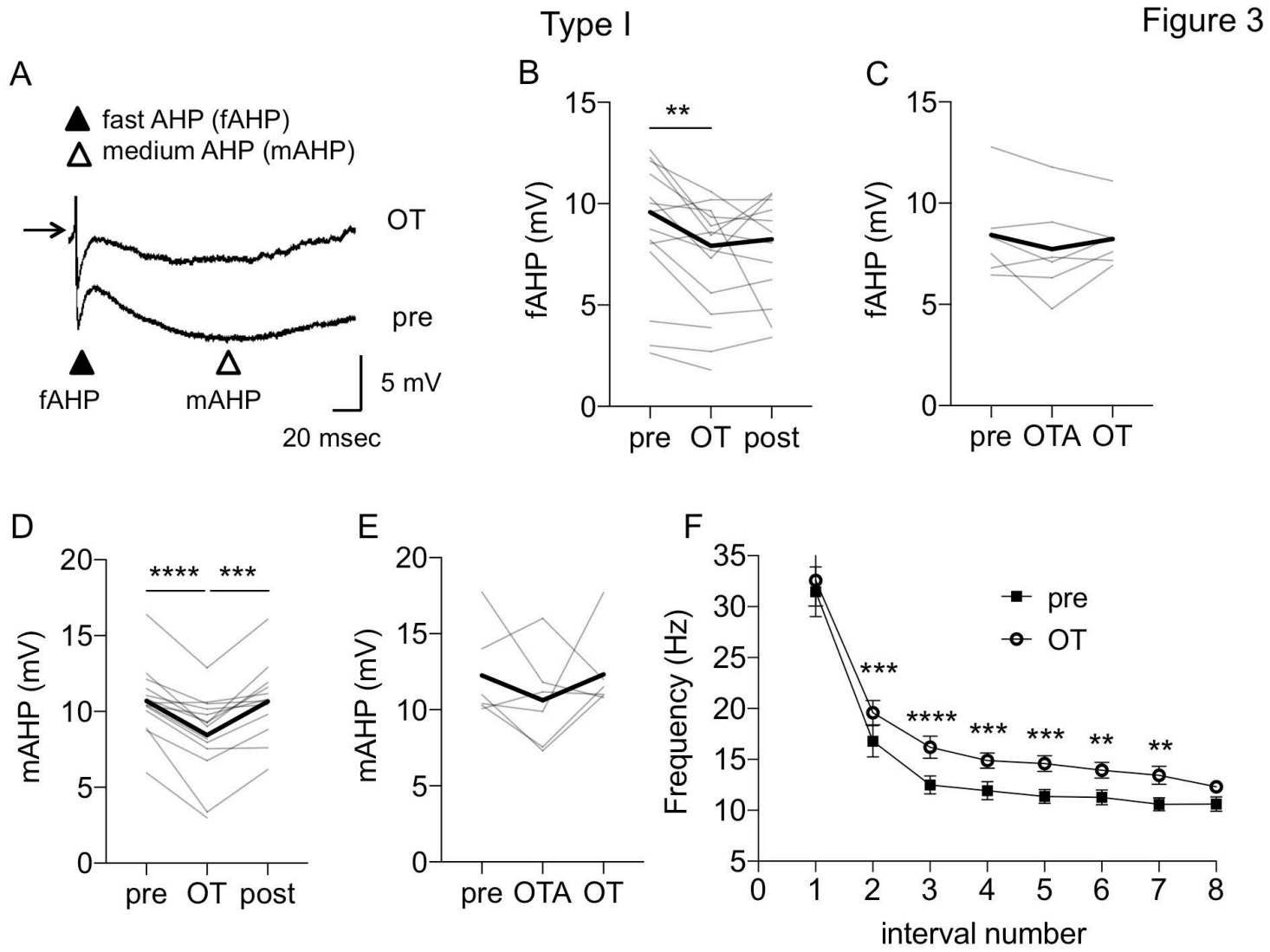

Figure 3. Oxytocin reduces fast and medium afterhyperpolarizations and modifies early and late spike frequency adaptation in Type I $BNST_{DL}$ neurons. **A**: A representative trace from Type I neuron showing a reduction of fast AHP (fAHP) and medium AHP (mAHP) after OT application respective to baseline (pre). The amplitudes of the fAHP and mAHP following the first action potential evoked at Rh were calculated as the difference from the action potential threshold to the membrane voltage measured after 2-5 msec and 50-100 msec, respectively. The lAHP was measured at 2000 msec after the end of the depolarizing pulse, following generation of five action potentials. **B**: Line graphs showing individual neurons' responses (gray) and reduction of the fAHP during OT application (P = 0.0124, F (1.473, 17.68 = 6.493, mixed-effects analysis, n = 14). **C**: OTR antagonist, OTA (0.4 μM), prevents the OT-induced reduction of fAHP (P = 0.2220, n = 7, RM one-way ANOVA). **D**: Line graph showing reduction of mAHP during OT application (P <0.0001, F (1.844, 22.13) = 23.25, mixed effect analysis, n = 14). **E**: OT-induced reduction of mAHP is blocked by OTR antagonist, OTA (P = 0.3968, n = 7, RM one-way ANOVA). Thick black lines show average responses for all Type I neurons recorded. **F**: OT modifies early and late spike frequency adaptation. The early and late spike frequency adaptation was investigated using a depolarizing pulse of 1 sec and measuring the instantaneous frequency for every action potential interval. The ISI number is the inter-stimulus interval between two consecutive action potentials. OT significantly increased the instantaneous frequency of ISI (P < 0.0001, F (1, 13) = 82.69, mixed effects model). Each data point represents the mean ± SEM, ****P < 0.0001, ***P < 0.001, **P < 0.01, *P < 0.05.

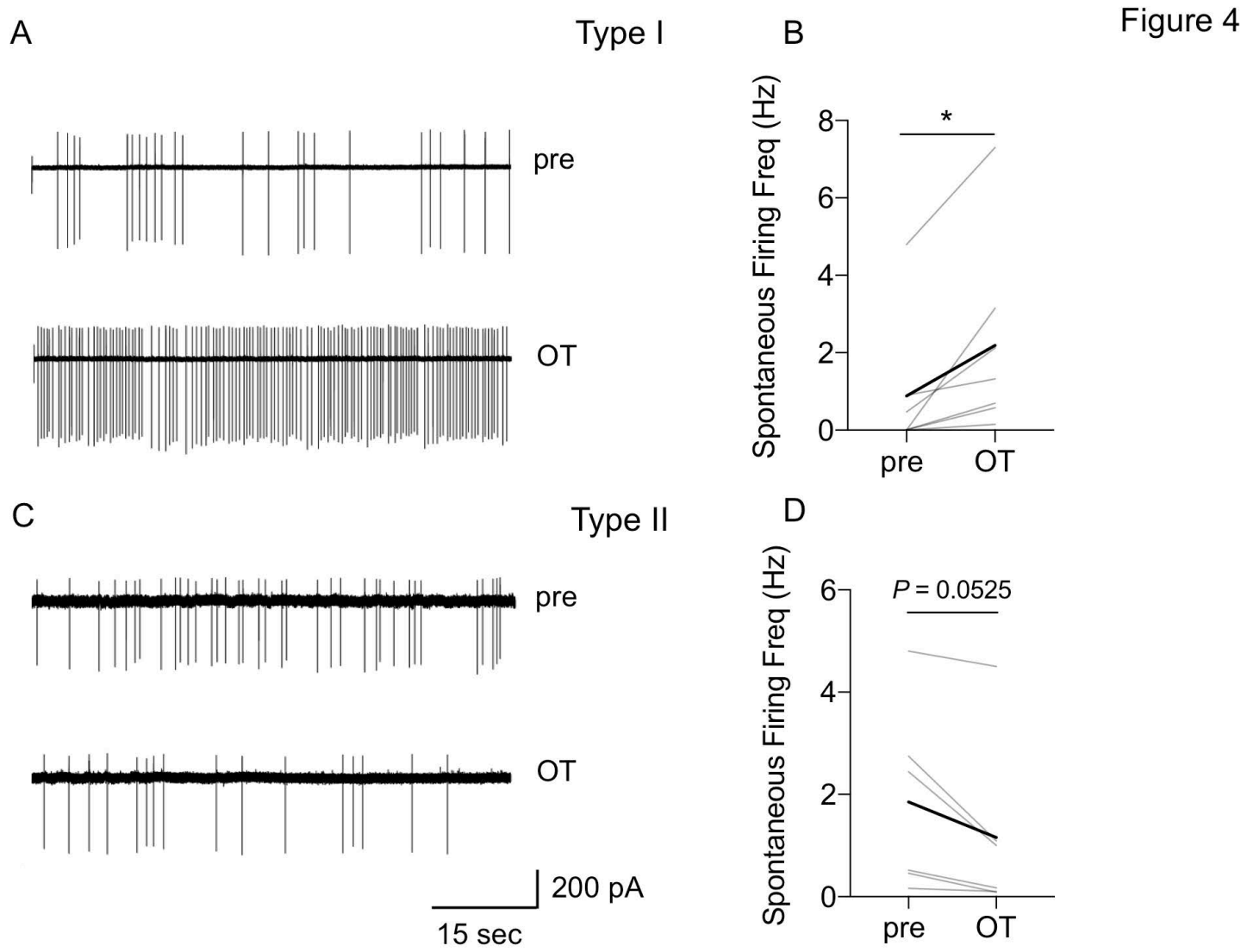

Figure 4. Oxytocin increases spontaneous firing rate of Type I neurons and reduces spontaneous firing rate of Type II $BNST_{DL}$ neurons in cell-attached recordings. **A**: A representative trace of Type I neuron showing an increase in spontaneous firing rate after OT application. **B**: Line graph showing that OT increased spontaneous firing rate in all spontaneously firing Type I neurons (P = 0.0242, paired t-test, n = 7), gray lines represent individual neurons' responses, thick black line represents average response. **C**: A representative trace of Type II neuron showing a reduction in spontaneous firing rate after OT application. **D**: Line graph showing that OT reduced spontaneous firing rate in spontaneously firing Type II neurons in cell-attached mode (P = 0.0525, paired t-test, n = 6).

177 ***2.2. The effects of OT on inhibitory synaptic transmission in Type I-III BNST$_{DL}$ neurons.***

178 To study the effect of OT on spontaneous inhibitory postsynaptic currents (sIPSCs), the
179 events were recorded from Type I-III neurons in a voltage clamp mode at holding potential of -
180 70 mV, in a presence of glutamatergic transmission's blockers. In Type II BNST$_{DL}$ neurons,
181 application of OT caused a significant increase in the frequency of sIPSCs in 12 out of 14
182 recorded neurons from 1.03 ± 0.20 Hz to 2.64 ± 0.47 Hz vs. baseline (pre, P = 0.0033), and vs.
183 washout (post, P = 0.0018, **Fig. 5A-B**). Notably, the effect of OT on the sIPSCs frequency was
184 not associated with a significant change in the amplitude (P = 0.9205, **Fig. 5C**) or in the total
185 charge (P = 0.5744, **not shown**). OT did not increase the sIPSCs frequency in the presence of
186 OTA (P = 0.3053**, Fig. 5D**). In addition, when the spike-driven sIPSCs were blocked (P =
187 0.0387) with Tetrodotoxin (TTX, 1 μM), OT no longer affected the frequency of miniature IPSCs
188 (mIPSCs) of Type II neurons (P = 0.9975, **Fig. 5E**). Finally, after electrical stimulation of the
189 Stria Terminalis, OT did not affect the evoked IPSCs (eIPSCs) amplitude (at the Vh of +10 mV)
190 in Type II neurons (from 266.76 ± 55.43 pA (pre) to 316.17 ± 82.49 pA, post, P = 0.2459, paired
191 *t*-test, **Fig. 6A-B**). These results demonstrate that OT indirectly increases the frequency of
192 spike-driven sIPSCs in Type II neurons.

193 In Type I neurons, OT did not affect the sIPSCs frequency (P = 0.3018), amplitude (P =
194 0.3347), or total charge (P = 0.6087, **not shown**). Moreover, OT did not change the amplitude
195 of the eIPSC in Type I neurons (P = 0.2449, **not shown**). In Type III neurons, OT did not affect
196 the frequency (P = 0.9440, **Fig. 5F**), but it reduced amplitude (P = 0.0314, **Fig. 5G**) and total
197 charge of sIPSCs (P = 0.0372, **not shown**). In Type III neurons, OT significantly reduced the
198 amplitude of the eIPSCs from 286.76 ± 97.41 (pre) to 210.69 ± 78.57 pA (P = 0.0105, paired *t*-
199 test, **Fig. 6C-D**). This reduction of the eIPSC amplitude was not associated with a significant
200 change in the paired pulse ratio (PPR) (P = 0.5672, paired *t*-test, **Fig. 6E**), suggesting that in
201 Type III neurons OT affects the synaptic response through a postsynaptic mechanism. Notably,

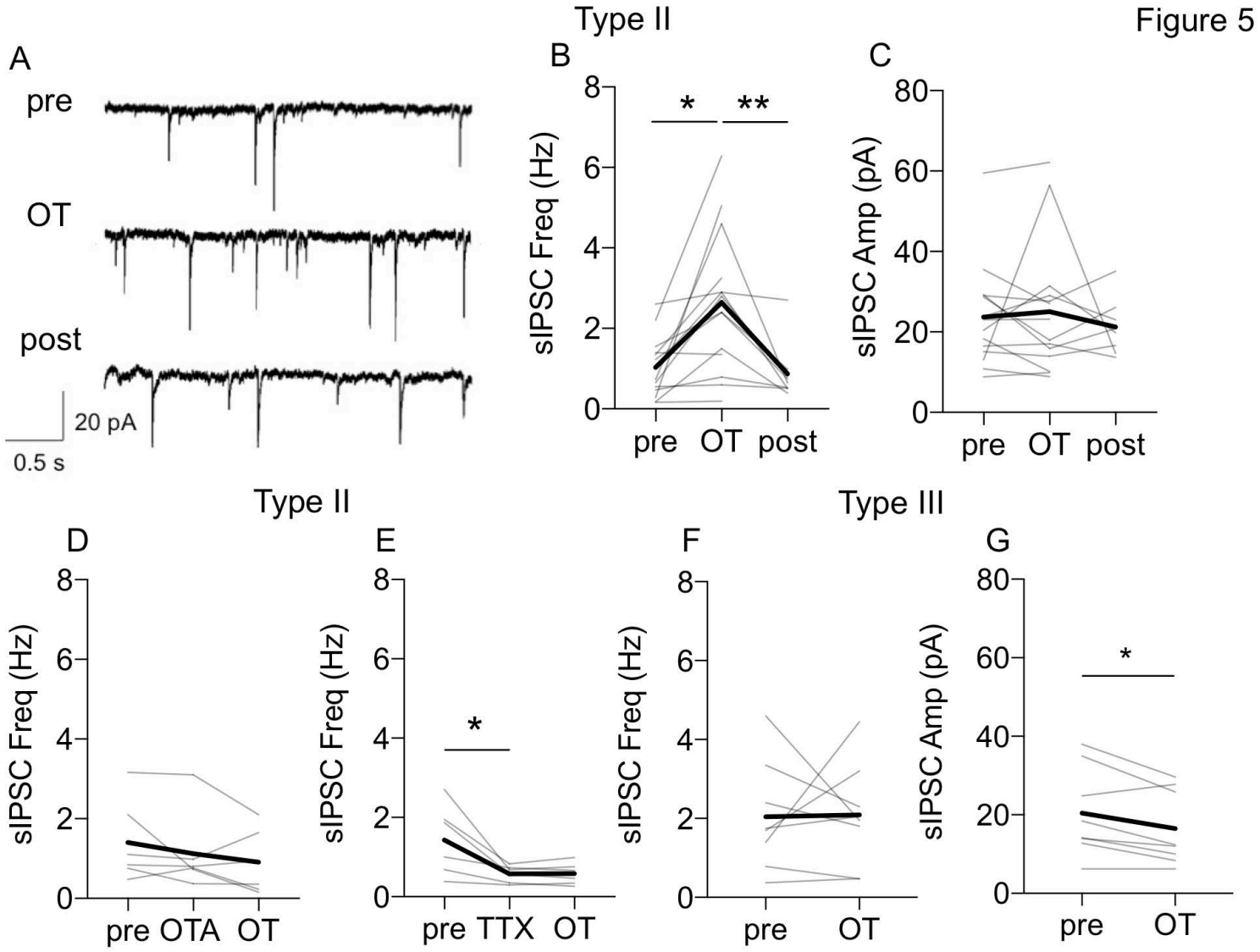

Figure 5. Oxytocin modulates inhibitory synaptic transmission in $BNST_{DL}$ neurons. **A**: Representative recordings showing an increase in the frequency of spontaneous inhibitory postsynaptic currents (sIPSCs) after OT application respective to baseline (pre). **B-C**: Line graphs (gray) showing that 12 out of 14 recorded Type II neurons showed an increase in sIPSCs frequency (**B**, $P = 0.0022$, F (1.058, 12.17) = 14.41, n = 14, mixed-effect analysis) but not amplitude (**C**, $P = 0.5855$, F (1.563, 17.19) = 0.4718, n = 14, mixed-effect analysis) after OT application. **D**: OT does not affect sIPSC frequency in a presence of OTR antagonist, OTA (0.4 μM) ($P = 0.1788$, F (1.469, 8.814) = 2.135, n = 6, RM ANOVA). **E**: When spike-driven IPSCs were blocked with TTX ($P = 0.0151$, F (1.030, 6.179) = 10.98, n = 6, RM ANOVA), OT does not affect the sIPSCs frequency. **F-G**: OT does not affect frequency (**F**, $P = 0.9362$) but reduces amplitude of sIPCS in Type III neurons (**G**, $P = 0.0160$, paired *t*-test). Thick black lines show averaged responses for all neurons recorded. Each data point represents the mean ± SEM, $^{**}P < 0.01$, $^{*}P < 0.05$ in comparison to pre- or post-OT.

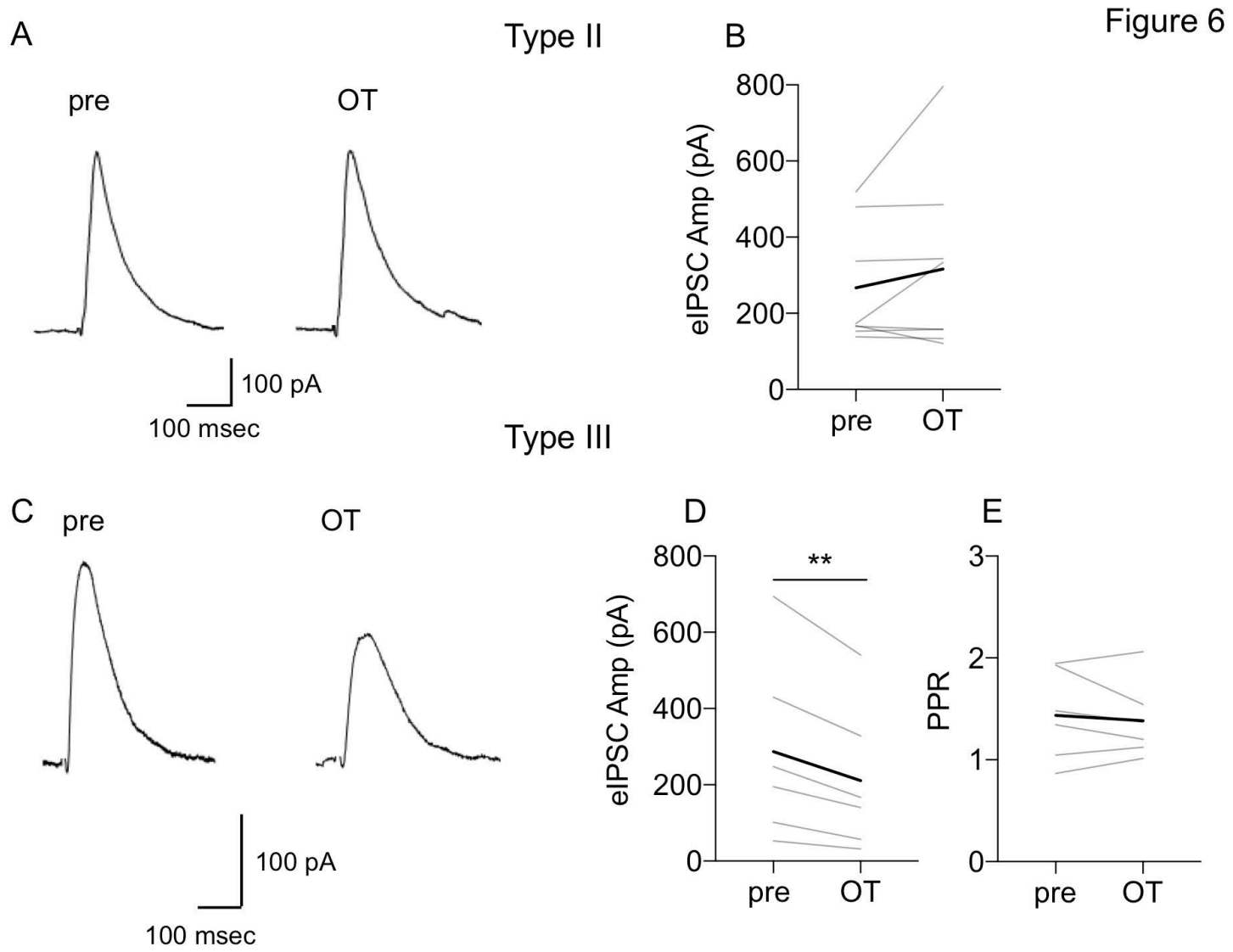

Figure 6. Oxytocin increases amplitude of evoked IPSCs in Type III, but not Type II $BNST_{DL}$ neurons. **A**: Representative traces of eIPSC in response to the electrical stimulation of the stria terminalis in Type II neurons. **B**: Line graph showing that OT does not significantly change the mean amplitude of eIPSC in Type II neurons (P = 0.2459, paired t-test). Thick black lines show averaged responses for all neurons recorded. **C**: Representative traces of eIPSCs in Type III neurons showing reduction of the eIPSCs amplitude after OT application. **D-E**: Line graphs showing individual Type III neurons and the reduction of the eIPSC amplitude after OT (**D**, P = 0.0105) without any significant change in the PPR (**E**, P = 0.5672).

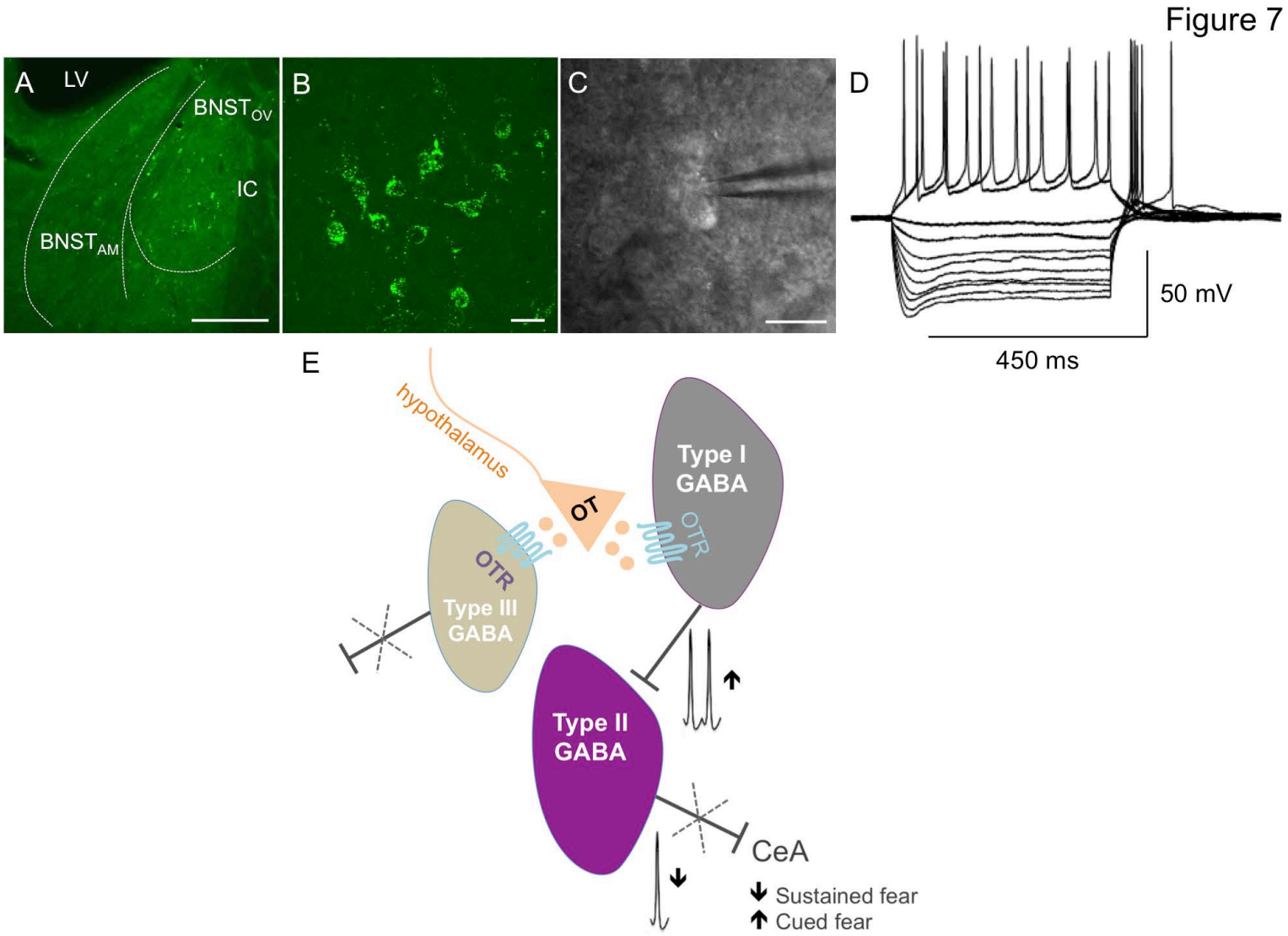

Figure 7. Type II neurons are output neurons of the BNST$_{DL}$ to the central amygdala. A-B: Microphotographs showing neurons expressing green fluorescent microbeads in the BNST$_{DL}$ after the retrobeads were injected into the central amygdala (CeA). **A**: BNST neurons projecting to the CeA (BNST⇒CeA neurons) were primarily found in the dorsolateral BNST, primarily the oval nucleus, BNST$_{OV}$, and to a lesser extent in the anteromedial BNST, BNST$_{AM}$ (20x, LV – Lateral ventricle, IC – Internal capsulae, scale bar 100 μm). **B**: High magnification (60x) microphotographs showing green fluorescent beads present in membranes and processes of the BNST⇒CeA neurons (scale bar 10 μm). **C-D**: Electrophysiological characterization of the BNST⇒CeA neurons using visually guided patching (**C**, 40x, scale bar 20 μm). Representative recording of the BNST⇒CeA fluorescent neuron showing the electrophysiological properties of a Type II neuron such as the presence of a sag during the hyperpolarized current pulses and the spike rebound at the end of the 450 ms current pulse injection (**D**). **E**: Diagram showing that OT regulates the intrinsic inhibitory network and inhibits output neurons of the BNST$_{DL}$. By directly increasing frequency of spontaneous firing of Type I regular spiking neurons, OT inhibits firing of Type II BNST$_{DL}$ neurons. Type II neurons are output neurons of the BNST$_{DL}$ sending projections to the CeA (BNST⇒CeA neurons). OT also inhibits another class of output neurons, Type III, via a direct postsynaptic mechanism. Therefore, OT excites BNST$_{DL}$ interneurons (Type I) and inhibits two distinct classes of the BNST$_{DL}$ projection neurons via indirect (Type II) and direct (Type III) mechanisms, respectively.

202 in a presence of OTR antagonist, OT did not reduce the amplitude of eIPSCs in Type III
203 neurons (*P* = 0.8286, **not shown**).

204 ***2.3. CeA-projecting $BNST_{DL}$ neurons***

205 To determine an electrophysiological phenotype of central amygdala-projecting $BNST_{DL}$
206 (*BNST➔CeA)* neurons, rats were first bilaterally injected into the CeA with a retrograde tracer,
207 green microbeads. Retro-labeled fluorescent neurons were found in subdivisions of the $BNST_{DL}$,
208 primarily in the oval nucleus of the $BNST_{DL}$ ($BNST_{OV}$) and to a lesser extent in anteromedial
209 BNST ($BNST_{AM}$, **Fig. 7A-B**). We found healthy fluorescent neurons that were suitable for
210 recordings in 6 out of 17 rats. In the slices from those 6 rats, we recorded 8 fluorescent neurons
211 in the $BNST_{OV}$ (**Fig. 7C**), and all recorded neurons were classified as Type II neurons (**Fig. 7D**).

212 **3. Discussion**

213 Here we demonstrate that OT regulates the intrinsic inhibitory network of the $BNST_{DL}$, where it
214 increases intrinsic excitability and spontaneous firing of Type I, regular spiking interneurons,
215 which leads to a potentiation of GABA-ergic inhibition and a reduction of spontaneous firing of
216 Type II, burst firing neurons. Using visually guided patching of retro-labeled $BNST_{DL}$ neurons,
217 we confirm that Type II are output neurons of the $BNST_{DL}$, which project to the CeA
218 (*BNST➔CeA* neurons). Furthermore, we show that OT inhibits another class of $BNST_{DL}$
219 projection neurons, Type III, via a direct postsynaptic mechanism. Therefore, we demonstrate
220 that there are three groups of OT-responsive neurons in the $BNST_{DL}$; a population of
221 interneurons (Type I) that is directly excited by OTR activation, and two distinct groups of
222 projection neurons, which are indirectly (Type II) and directly (Type III) inhibited by OT (**Fig. 7E).**
223 The OT-mediated inhibition of the $BNST_{DL}$ output has powerful implications for the modulation of
224 fear and anxiety-like behaviors.

225 Neurons of the $BNST_{DL}$ are GABA-ergic (Cullinan et al., 1993; Dabrowska et al., 2013a;
226 Sun and Cassell, 1993), and can be categorized into three major types (I-III) (Daniel et al.,
227 2017; Hammack et al., 2007). Type I neurons, characterized by regular firing and lack of burst-

228 firing activity (Hammack et al., 2007; Hazra et al., 2011), were classified as interneurons by
229 Paré and colleagues (Rodríguez-Sierra et al., 2013). This has been recently supported by
230 retrograde labeling showing a very small fraction of Type I neurons (in comparison to Type II
231 and Type III) projecting outside of the $BNST_{DL}$ (Yamauchi et al., 2018). We show that Type I
232 neurons are the primary OT-responsive neurons of the $BNST_{DL}$ as demonstrated by their
233 increased excitability and spontaneous firing rate after OT application. Previous studies using
234 single unit recordings showed that OT increased the spontaneous firing rate of 50% of BNST
235 neurons in lactating female rats (Ingram et al., 1990), and the magnitude of the response was
236 significantly potentiated during lactation (Ingram and Moos, 1992). Notably, in our study, the
237 excitatory effects of OT in Type I neurons are paralleled by increased inhibitory transmission
238 observed in Type II $BNST_{DL}$ neurons. The specific effect of OT on the sIPSCs frequency, but not
239 amplitude, suggests a presynaptic mechanism in Type II neurons. In addition, since the effect
240 was no longer observed when the spike-driven IPSCs were suppressed with TTX, this indicates
241 an indirect influence driven by an increased spontaneous firing of $BNST_{DL}$ interneurons. This
242 has been further supported by the lack of the OT effect on eIPSCs in Type II neurons,
243 suggesting that the inhibitory effect of OT in Type II neurons is not a result of the stimulation of
244 the extrinsic inhibitory projections.

245 In contrast, in Type III neurons, OT reduced the amplitude and the total charge, but not
246 the frequency of sIPSCs, as well as reduced the amplitude of eIPSC without changing the PPR,
247 overall indicating a postsynaptic effect. OT was shown previously to depress GABA-ergic
248 synapses in the supraoptic nucleus of the hypothalamus via postsynaptic increase of Ca^{2+} due
249 to the activation of G-protein coupled receptors (Alger and Nicoll, 1980; Brussaard et al., 1996).
250 However, since in our hands the effect on the amplitude was accompanied by a reduction in the
251 total charge, this could potentially indicate shortening of GABA channel opening (Martina et al.,
252 1994) via OTR-mediated increases in intracellular Ca^{2+}, as demonstrated after OTR activation
253 before (Brussaard et al., 1996). Therefore, in Type III neurons OT might reduce the amplitude of

254 sIPSCs and eIPSC through a postsynaptic mechanism involving signal transduction-mediated
255 regulation of intracellular Ca^{2+} levels. In addition, direct inhibitory effect of OT mediated via OTR
256 linked to inhibitory Gi-subunit was demonstrated in sensory neurons of spinal cord before
257 (Eliava et al., 2016).

258 To further investigate the OT effects on intrinsic excitability and firing, we demonstrated
259 that OT reduced fAHP and mAHP selectively in Type I neurons. AHPs generated after a single
260 action potential or a train of action potentials limit the frequency of neuronal firing (Alger and
261 Nicoll, 1980), as demonstrated by a significant increase in action potential firing after
262 pharmacological inhibition of AHPs (Pedarzani and Storm, 1993). The fAHP, mediated by BK
263 channels, is responsible for early spike frequency adaptation in many neuronal types (Gu et al.,
264 2007). The mAHP is mediated by the non-inactivating M-current, which blockade with selective
265 antagonist reduces late spike adaptation (Gu et al., 2008, 2005b). An OTR-mediated increase of
266 neuronal excitability was recently shown in the hippocampus, where a selective OTR agonist
267 induced membrane depolarization and increased membrane resistance in CA2 pyramidal cells
268 leading to a leftward shift in their firing frequency-current relationship (Tirko et al., 2018). Here
269 we show that OT-mediated excitation of Type I neurons in the $BNST_{DL}$ was associated with a
270 significant increase in instantaneous frequency of action potentials due to the reduction in the
271 early and late adaptation. Therefore, by acting on potassium conductances OT might increase
272 the intrinsic excitability and the spontaneous firing of Type I neurons.

273 According to our knowledge, this is the first study utilizing cell-attached mode in a cell-
274 type specific manner to show that in the $BNST_{DL}$, the majority of Type I neurons fire
275 spontaneously, and this effect is further potentiated by OT. Notably, although we showed that
276 the majority of Type II neurons remain silent even during cell-attached configuration, in all
277 spontaneously firing Type II neurons, OT application reduced the rate of firing. Notably, the
278 indirect inhibitory effect on spontaneous firing of Type II neurons was further confirmed by the
279 lack of the OT effect on current-evoked firing in these neurons, which was investigated in a

280 presence of synaptic transmission blockers. The latter further suggests that OT does not alter
281 intrinsic properties of Type II neurons and instead, reduces the spontaneous firing rate and so
282 their inhibitory synaptic transmission via the direct excitatory effect on Type I neurons.

283 The BNST was not entirely isolated during recordings, such as the slice also potentially
284 contained GABA-ergic neurons in the medial preoptic area (Okamura et al., 1990), which
285 express OTR (Sharma et al., 2019), and project to the BNST (Simerly and Swanson, 1988).
286 However, this projection primarily targets the principal encapsulated nucleus in the posterior
287 BNST (Maejima et al., 2015), where OTR are involved in reproductive behavior (Kremarik et
288 al., 1991). Notably, the posterior BNST was not a part of our slice preparation. In addition,
289 although we cannot entirely rule out a possibility that some inhibitory inputs to the $BNST_{DL}$ might
290 be originating from anteromedial ($BNST_{AM}$) or ventral BNST ($BNST_{VEN}$), which were included in
291 our slice, the intrinsic inhibitory projections in the BNST have been primarily shown to originate
292 in the $BNST_{DL}$, mainly the $BNST_{OV}$, and target $BNST_{AM}$ and $BNST_{VEN}$, whereas opposite
293 projections are rare (Gungor and Paré, 2016). Therefore, our results strongly suggest that Type
294 I neurons are $BNST_{DL}$ interneurons providing inhibitory synaptic input to Type II neurons, an
295 effect potentiated by OT.

296 It is important to note that the BNST also contains neurons producing arginine-
297 vasopressin (AVP) (al-Shamma and De Vries, 1996) and has a high expression of AVP
298 receptors, V1AR (Grundwald et al., 2016). As OT shows a relatively high affinity toward AV1R,
299 this raises a possibility of non-specific effects via V1AR. However, all the significant OT effects
300 in our study were blocked by OTA, which is highly selective toward OTR with a negligible affinity
301 toward V1AR, see (Manning et al., 2012).

302 Similar modulation of the intrinsic inhibitory network by OT was shown in a variety of
303 limbic brain regions, including the CeA. The CeA and the BNST share many similarities,
304 including predominantly GABA-ergic nature, analogous peptidergic cell types, as well as similar
305 intrinsic and extrinsic connectivity, and together they form an extended amygdala complex

306 (Alheid, 2003; Sun and Cassell, 1993). Interestingly, in the CeA, there are two groups of OT-
307 responsive neurons. A group of interneurons located in the lateral nucleus of the CeA (CeL)
308 (Gozzi et al., 2010) is excited by OTR activation (Huber et al., 2005; Terburg et al., 2018; Viviani
309 et al., 2011). Once excited by OT, these interneurons provide inhibitory input to medial nucleus
310 of the CeA (CeM) output neurons, which were shown to selectively project to lateral
311 periaqueductal gray and reduce contextual fear (Viviani et al., 2011), for review see (Beyeler
312 and Dabrowska, 2020). Similarly to the effects we observed in the $BNST_{DL}$, OTR-mediated
313 indirect inhibition of the CeM output neurons was demonstrated as increased frequency of
314 sIPSC during whole-cell recordings and reduced spontaneous firing rate in a cell-attached
315 configuration. Similarly, in the hippocampus (Harden and Frazier, 2016; Maniezzi et al., 2019;
316 Owen et al., 2013; Tirko et al., 2018; Zaninetti and Raggenbass, 2000), lateral amygdala (Crane
317 et al., 2020), and the prefrontal cortex (Marlin et al., 2015; Nakajima et al., 2014), OT was
318 shown to excite a population of interneurons, including fast-spiking parvalbumin interneurons,
319 which were shown to inhibit glutamatergic projection neurons.

320 We show that in the $BNST_{DL}$, OT inhibits two classes of projection neurons via indirect
321 (Type II) and direct (Type III) mechanisms. Recently, both Type II and Type III were
322 demonstrated output neurons of the $BNST_{DL}$, with major projections to the CeA (62% of Type II
323 and 33% of Type III), LH (83% of Type III), and the VTA (17% of Type II, 79% of Type III
324 neurons). Although at this time we cannot unequivocally state that OT specifically inhibits the
325 *BNST➔CeA* neurons, OT increased the sIPSCs frequency and reduced the spontaneous firing
326 in 86% and 100% of recorded Type II neurons, respectively. In addition, all the retrogradely
327 labeled *BNST➔CeA* neurons we recorded from the $BNST_{OV}$ were identified as Type II.
328 Therefore, there is a high probability that OT inhibits the *BNST➔CeA* neurons. It would still
329 need to be determined whether OT inhibits specific Type III projection neurons. Although
330 neuropeptidergic phenotypes corresponding to Type I-III neurons remain elusive, Type III are
331 putative corticotropin-releasing factor (CRF) neurons of the $BNST_{OV}$ (Dabrowska et al., 2013b)

332 and they were shown projecting to the LH, VTA, and the CeA, among many other brain regions
333 (Dabrowska et al., 2016).

334 Notably, Type II neurons are the most abundant and heterogeneous neuronal population
335 in rat $BNST_{DL}$ (Hazra et al., 2011; Yamauchi et al., 2018). Although the projection from the
336 $BNST_{DL}$ to the CeA has been shown before (McDonald et al., 1999), a functional inhibitory
337 projection was recently demonstrated using optogenetics (Gungor et al., 2015; Yamauchi et al.,
338 2018). The BNST is known to mediate stress-induced anxiety-like responses (Dabrowska et al.,
339 2013b; Daniel and Rainnie, 2016; Davis et al., 2010; Sparta et al., 2013), contextual fear (Davis
340 et al., 2010; Sullivan et al., 2004; Waddell et al., 2006), as well as fear responses to un-
341 signaled, diffuse, or unpredictable threats (Duvarci et al., 2009; Goode et al., 2020, 2019). The
342 recent optogenetic study showed that activation of the *BNST➔CeA* projection increases
343 anxiety-like behavior (Yamauchi et al., 2018), suggesting that the *BNST➔CeA* neurons are
344 important output neurons recruited during heightened states of anxiety. In addition, the BNST
345 has been shown to inhibit cued fear responses to discrete threats (Meloni et al., 2006). Notably,
346 our recent behavioral studies have demonstrated that OTR transmission in the $BNST_{DL}$
347 facilitates acquisition of cued fear and reduces fear responses to un-signaled/diffuse threats
348 (Janeček and Dabrowska, 2019; Martinon et al., 2019; Moaddab and Dabrowska, 2017),
349 showing opposite effects to the effects of the BNST activation. Our current electrophysiology
350 results suggest that OTR activation in the $BNST_{DL}$ facilitates cued fear and reduces anxiety by
351 inhibiting the *BNST➔CeA* output neurons.

352 ***4. Material and methods***

353 ***4.1. Animals***

354 Male Sprague-Dawley rats (Envigo, Chicago, IL; 240-300 g) were housed in groups of three on
355 a 12 h light/dark cycle (light 7 a.m. to 7 p.m.) with free access to water and food. Rats were
356 habituated to this environment for one week before the experiments began. Experiments were
357 performed in accordance with the guidelines of the NIH and approved by the Animal Care and

358 Use Committee at RFUMS. A total of 144 rats were used for the experiments. The effects of OT
359 on membrane properties were tested in 14 Type I neurons (from 10 rats), 13 Type II (12 rats),
360 and 9 Type III neurons (8 rats). The effect of OT on evoked firing was tested on 12 Type I (11
361 rats), 8 Type II (7 rats), and 9 Type III neurons (8 rats). The effect of OT on the spontaneous
362 firing was tested in 9 Type I (8 rats) and 18 Type II (15 rats). To study the effect of OT on
363 sIPSCs, we recorded 14 Type II (12 rats), 6 Type I (5 rats), and 8 Type III neurons (8 rats). We
364 recorded 6 Type II neurons (4 rats) in experiment with OTR antagonist, and 6 Type II neurons (5
365 rats) in TTX experiment. The effect of OT on the evoked IPSCs was tested in 5 Type I (5 rats), 8
366 Type II (8 rats), and 6 Type III (5 rats) neurons. We recorded 5 Type III (4 rats) neurons in
367 experiments with OTR antagonist. We recorded 8 retrogradely labeled Type II neurons (17 rats).

368 ***4.2. Slice preparation for electrophysiology***

369 Rats were anaesthetized with Isoflurane USP (Patterson Veterinary, Greeley, CO, USA) before
370 decapitation. Brains were quickly removed and coronal 300 μm slices containing the $BNST_{DL}$
371 were prepared in ice-cold cutting solution (saturated with 95% O_2/ 5% CO_2) containing in mM:
372 NaCl 130, KCl 3.5, $NaHCO_3$ 30, KH_2PO_4 1.1, $CaCl_2 \cdot 2H_2O$ 1, D-glucose 10, $MgCl_2$ $6H_2O$ 6,
373 Kynurenate 2, pH 7.4, 290-300 mOsm. The slices were prepared using a Leica vibratome
374 (VT1200; Leica, Wetzlar, Germany), then incubated for 1 hr at 34°C in the cutting solution and
375 subsequently transferred to room temperature in artificial cerebrospinal fluid (aCSF) containing
376 in mM: NaCl 130, KCl 3.5, $NaHCO_3$ 30, KH_2PO_4 1.1, $CaCl_2 \cdot 2H_2O$ 2.5, D-glucose 10, and
377 $MgCl_2 \cdot 6H_2O$ 1.3, Ascorbate 0.4, Thiourea 0.8, Na Pyruvate 2, pH 7.4, with osmolarity of 290-300
378 mOsm, continuously oxygenated with 95% O_2/ 5% CO_2. Next, the slices were transferred to a
379 submerged recording chamber and perfused with aCSF at 33°C ± 1°C saturated with 95% O_2/
380 5% CO_2 at a flow rate of 2-3 ml/min. $BNST_{DL}$ neurons were visualized using infrared differential
381 interference contrast (IR-DIC) optic with an Upright microscope (Scientifica SliceScope Pro
382 1000, Clarksburg, NJ, USA).

383 ***4.3. Patch-clamp recordings***

384 Whole-cell patch-clamp recordings were performed from $BNST_{DL}$ neurons, primarily in the oval
385 nucleus of the BNST ($BNST_{OV}$), using glass pipette (4-8 MΩ) pulled from thick-walled
386 borosilicate glass capillaries with a micropipette puller (Model P-97; Sutter Instrument, Novato,
387 CA, USA) as before (Dabrowska et al., 2013b; Francesconi et al., 2009). To study the effects of
388 OT (0.2 μM concentration based on (Crane et al., 2020; Xiao et al., 2017), oxytocin acetate salt,
389 # H-2510, Bachem, Switzerland) on intrinsic membrane properties and firing activity the patch
390 pipettes were filled with potassium gluconate internal solution containing in mM: K-gluconate
391 135, KCl 2, $MgCl_2 \cdot 6H_2O$ 3, HEPES 10, Na-phosphocreatine 5, ATP-K 2, GTP-Na 0.2, pH 7.3
392 adjusted with KOH, 300-305 mOsm. Intrinsic membrane properties experiments were performed
393 in a presence of synaptic transmission blockers: the AMPA receptor antagonist CNQX (10 μM),
394 the NMDA receptor antagonist AP-5 (50 μM), and GABA-A receptor antagonist, picrotoxin (25
395 μM). To study the effects of OT on the spontaneous inhibitory postsynaptic currents (sIPSCs),
396 the patch pipettes were filled with high chloride internal solution in mM: KOH 110, $MgCl_2 \cdot 6H_2O$
397 2, KCl 50, EGTA 0.2, ATP-Na 2, GTP-Na 0.3, HEPES 10, and Spermine 0.1, the pH was
398 adjusted to 7.3 with D-gluconic acid and osmolarity was 300-305 mOsm. The evoked IPSCs
399 (eIPCSs) were recorded with pipettes filled with K-gluconate solution as described above. In
400 order to isolate GABAergic eIPSCs, the eIPSCs were recorded at the holding voltage (Vh) of
401 +10 mV, which is the reversal potential for the excitatory postsynaptic current. A stimulating
402 pipette filled with aCSF was placed in the Stria Terminalis. For each neuron recorded the
403 stimulus intensity was adjusted to give an eIPSCs of about 1/3 of the maximal amplitude and
404 maintained throughout the experiment. We applied 10 paired pulse stimuli (ISI 50 msec) at the
405 frequency of 0.2 Hz. The peak amplitude of the eIPSC was measured from the averaged
406 responses. The responses were acquired each minute for 10 min before and 12 min after OT
407 application. The paired pulse stimulus was used to calculate the PPR between the mean
408 amplitude of the second eIPSC divided by the amplitude of the first eIPSC. Here we used the

409 PPR to evaluate a possible presynaptic mechanism of the OT effect on the BNST neurons
410 inhibitory synaptic responses.

411 To verify that the effects of OT were mediated by OTRs, selective and potent OTR
412 antagonist d(CH2)5(1), D-Tyr(2), Thr(4), Orn(8), des-Gly-NH2(9)]-Vasotocin trifluoroacetate salt
413 (Manning et al., 2012) (0.4 μM, OTA, V-905 NIMH Chemical Repository) was applied 10 min
414 before OT in all whole-cell experiments. Recordings were performed with a Multiclamp 700B
415 amplifier (Molecular Device, Sunnyvale, CA, USA). Current-clamp and voltage-clamp signals
416 were acquired at 10 kHz with a 16-bit input-output board NI USB-6251 (National Instruments,
417 Austin, TX) using custom MatLab scripts (Math-Work, Natick, MA) written by Dr. Niraj Desai
418 (Desai et al., 2017). All neurons included in the analysis had a seal resistance > 1GΩ and an
419 initial access resistance < 20 MΩ maintained for the entire recording period. Any cells showing
420 a 10% change in the serial resistance were not included in the analysis.

421 ***4.3.1. Electrophysiological characterization of $BNST_{DL}$ neurons***

422 Type I neurons are regular firing and display spike frequency adaptation. These neurons also
423 display moderate voltage sag that indicates the presence of the hyperpolarization-activated
424 cation current (I_h). As a distinguishing feature of Type II neurons, post-inhibitory spikes are
425 produced in response to preceding negative current steps that are related to the action of the
426 low-threshold Ca^{2+} current. Additionally, Type II neurons display strong voltage sags under
427 hyperpolarizing current pulses that indicate a high level of I_h current. Type III neurons differ from
428 the previous two types in several aspects: they exhibit high rheobase and no voltage sag under
429 negative current steps; they display prominent inward rectification that is caused by the
430 activation of the inward rectifying K^+ current (I_{KIR}) at membrane potentials more negative than
431 approximately −50 mV; and start firing after a characteristic slow voltage ramp mediated by the
432 K^+ delayed current (I_D).

433 ***4.3.2. Cell-attached recordings***

434 The spontaneous firing activity of Type I and II $BNST_{DL}$ neurons was recorded in a cell-attached
435 voltage-clamp mode, using patch pipettes filled with K-gluconate solution as described above,
436 without blockers of the synaptic transmission. To avoid a possible effect of amplifier-generated
437 currents on the spontaneous firing activity during the recording the command potential was
438 carefully adjusted at the value at which no current was flowing from the amplifier through the cell
439 membrane as described by (Perkins, 2006). At the end of the spontaneous firing recording
440 period, a gentle negative pressure was applied to break through the membrane into whole cell
441 configuration and determine the neuron type in a current-clamp mode as described above.

442 ***4.3.3. The effect of OT on intrinsic membrane properties and spontaneous firing of Type***
443 ***I-III $BNST_{DL}$ neurons***

444 The amplitudes of the fAHP and mAHP following the first action potential evoked at Rh
445 were calculated as the difference from the action potential threshold to the membrane voltage
446 measured after 2-5 msec and 50-100 msec, respectively. The lAHP was measured at 2000
447 msec after the end of the depolarizing pulse, following generation of five action potentials. As
448 the K^+ currents underlying these AHPs are considered to regulate spike frequency adaptation
449 (Gu et al., 2008; Lopez de Armentia and Sah, 2004), we measured early and late spike
450 frequency adaptation before and after OT application using a depolarizing pulse of 1 sec. We
451 measured the spike frequency adaptation rather than the spike frequency, because the firing of
452 the BNST neurons, as described by Paré and colleagues (Rodríguez-Sierra et al., 2013), is
453 adapting and not regular. This is a characteristic of all types of $BNST_{DL}$ neurons, including Type
454 I (described as regular firing), which also adapt on a long current pulse. We also performed
455 recordings in cell-attached mode in Type I-II neurons and measured the spontaneous firing
456 frequency before and after OT. The spontaneous firing frequency (Hz) was determined as the
457 number of spontaneous spikes for every minute of recording.

458 ***4.3.4. The effect of OT on inhibitory synaptic activity of Type I-III $BNST_{DL}$ neurons***

459 To study the effect of OT on spontaneous inhibitory postsynaptic currents (sIPSCs), the events
460 were recorded from Type I-III neurons in a voltage clamp mode at holding potential of -70 mV.
461 To isolate the sIPSCs, the recordings were made in the presence of the AMPA receptor
462 antagonist CNQX (10 μM) and the NMDA receptor antagonist AP-5 (50 μM). The sIPSCs were
463 characterized by their mean frequency, amplitude, and charge (calculated as the area under the
464 curve) using custom scripts in MatLab. To reach an adequate number of events, the sIPSCs
465 were acquired continuously in 2-minute sweeps during the entire recording time. The sIPSCs
466 were recorded for 10 min in aCSF, followed by 12 min bath application of OT and followed by
467 the drug washout (at least 10 more min after the OT application was completed). As sIPSCs are
468 a combination of spike-independent IPSCs and spike-driven IPSCs, in some experiments the
469 action potential generation was blocked with Tetrodotoxin (TTX, 1 μM, #1078; Tocris
470 Bioscience, UK), leaving only the spike-independent IPSCs (miniature IPSCs, mIPSCs). $GABA_A$
471 receptor antagonist, picrotoxin (25 μM), was used at the end of the recordings to verify the
472 GABA-ergic origin of the sIPSCs. Finally, to study the effect of OT on the evoked inhibitory
473 synaptic transmission in Type I-III neurons, we recorded the eIPSCs by electrical stimulation of
474 the Stria Terminalis.

475 ***4.3.5. CeA-projecting $BNST_{DL}$ neurons***

476 To determine an electrophysiological phenotype of *BNST➔CeA* neurons, rats were first
477 bilaterally injected into the CeA with a retrograde tracer, green microbeads (Lumafluor Inc., 100
478 nl; AP: -2.4 mm, ML: +4.2 mm, DV: -8.2 mm), and were allowed to recover for 4-7 days before
479 electrophysiological recordings. Stereotaxic surgeries were performed as before (Martinon et
480 al., 2019; Moaddab and Dabrowska, 2017). The slices were illuminated with CoolLED pE-
481 300lite (Scientifica Ltd., Uckfield, UK) and ET - EGFP (FITC/Cy2) filter (Chroma Technology
482 Corp, Bellows Falls, VT, US) to enable visually guided patching of fluorescent neurons. Slices
483 were stored in 10% stabilized formalin post-recordings, mounted with Krystalon Mounting
484 medium (Millipore Sigma, #64969-71), and analyzed with Nikon Eclipse E600 microscope

485 (Melville, NY, US) and Olympus Fv10i confocal microscope for high magnification imaging
486 (Center Valley, PA, US).

487 **4.4. Statistical analysis**

488 All data are presented as MEAN ± standard error of mean (SEM). Distribution of data sets was
489 first evaluated with Kolmogorov-Smirnov test. Based on the normal distribution, the effects of
490 OT on the sIPSCs, excitability, and firing frequency were analyzed by a repeated measures
491 (RM) one-way analysis of variance (ANOVA) or mixed effects model, or paired *t*-tests, when
492 applicable. Where the F-ratio was significant, all-pairwise post hoc comparisons were made
493 using Tukey's or Sidak's tests. The statistical analyses were completed using GraphPad Prism
494 version 8.4.1 (GraphPad Software Inc., San Diego, CA). $P < 0.05$ was considered significant.

495 **5. Acknowledgements**

496 We would like to thank Dr. Attilio Caravelli for his help with Matlab. We also thank Rachel
497 Chudoba for proofreading the manuscript. This work was supported by grant from the National
498 Institute of Mental Health R01MH113007 and R01MH113007-04S1 to JD and start-up funds
499 from the Chicago Medical School, Rosalind Franklin University of Medicine and Science to JD.

500 **6. Contributions**

501 JD conceived the study. JD and WF designed the study. WF, FB, and VOP acquired data. WF,
502 FB, VOP, and JD analyzed data. WF, FB, VOP and JD interpreted data. JD and WF wrote the
503 manuscript. JD obtained funding.

504 **7. Financial Disclosures**

505 The authors declare no conflict of interest and have no financial interests to disclose. Dr.
506 Joanna Dabrowska reports submission of a provisional patent application entitled: Method and
507 System for Testing for Stress-related Mental Disorders, Susceptibility, Disease Progression,
508 Disease Modulation and Treatment Efficacy (# 62/673447).

509 **8. Figure legends**

510 **Figure 1. Oxytocin affects intrinsic membrane properties of Type I $BNST_{DL}$ neurons. A**: A
511 representative trace showing that oxytocin (OT, 0.2 μM) shortens the latency to the 1st spike at
512 rheobase current (Rh) and depolarizes resting membrane potential (RMP, from -64 mV to -60
513 mV). This is associated with increased input resistance (Rin), measured with a depolarizing
514 current step below the Rh. OT also reduces Rh from 30 pA (pre) to 20 pA (OT) **B-D**: Line
515 graphs with individual neurons' responses (thin gray) and average responses for all neurons
516 recorded (thick black) showing that OT significantly increases the RMP (**B**, P = 0.0002, F
517 (1.593, 19.12) = 15.76, n = 14, mixed-effect analysis), increases Rin (**C**, P = 0.0085, n = 9,
518 paired *t*-test), reduces the Rh (**D**, P = 0.0457, F (1.341, 16.09) = 4.226, n = 14, mixed-effect
519 analysis), reduces the 1st spike threshold (**E**, P = 0.0164, F (1.472, 20.61) = 5.749, and reduced
520 the 1st spike latency (**F**, P = 0.0185, F (1.971, 23.66) = 4.775, n = 14, mixed-effect analysis).
521 Thick black lines show average responses for all Type I neurons recorded. Each data point
522 represents the mean ± SEM, $^{**}P < 0.01$, $^{*}P < 0.05$ in comparison to pre or post-OT.

523 **Figure 2. Oxytocin increases intrinsic excitability of Type I, but not Type II or Type III,**
524 **$BNST_{DL}$ neurons**. **A**: A representative trace showing voltage deflections in response to
525 hyperpolarizing and depolarizing current injections characteristic of Type I neuron (left) and the
526 increase in firing frequency of Type I neuron in the presence of OT respective to baseline (pre)
527 (right). **B**: OT causes a leftward shift of input/output (I-O) relationship in Type I neurons. The
528 steady state frequency (SSF) was determined as an average of an inverse of the inter-spike
529 intervals (ISI) from all action potentials starting from the second action potential. In Type I
530 neurons***,*** OT shows a significant increment effect on SSF at 40 pA (P = 0.0024, F (1.667, 15.01)
531 = 10.11), at 50 pA (P = 0.0271, F (1.863, 16.76) = 4.628), and at 60 pA (P = 0.0271, F (1.688,
532 11.82) = 5.267, mixed-effects analysis). **C**: Application of OTR antagonist, OTA (0.4 μM),
533 prevents the leftward shift of the I-O relationship induced by OT application (40 pA, P = 0.3365,
534 50 pA, P = 0.4299, 60 pA, P = 0.6312, n = 5, RM ANOVA). **D-E:** OT application does not modify
535 the I-O relationship in Type II (**D**) or Type III $BNST_{DL}$ neurons (**E**). In Type II neurons, OT did not
536 affect SSF at 80 pA (P = 0.3116), 70 pA (P = 0.8236), 60 pA (P = 0.9519), 50 pA (P = 0.8993),

537 40 pA (*P* = 0.7636), 30 pA (*P* = 0.8673), or at 20 pA (*P* = 0.6990, **D**). Similarly, in Type III
538 neurons, there was no effect of OT on SSF at 80 pA (*P* = 0.1151), 70 pA (*P* = 0.1138), 60 pA (*P*
539 = 0.180), 50 pA (*P* = 0.0847), 40 pA (*P* = 0.1041), 30 pA (*P* = 0.0790), or at 20 pA (*P* = 0.0681,
540 **E**). Each data point represents the mean ± SEM, ***P* < 0.01, **P* < 0.05 in comparison to pre-OT,
541 ## *P* < 0.01, # *P* < 0.05 in comparison to post-OT.

542 **Figure 3. Oxytocin reduces fast and medium afterhyperpolarizations and modifies early**
543 **and late spike frequency adaptation in Type I $BNST_{DL}$ neurons**. **A**: A representative trace
544 from Type I neuron showing a reduction of fast AHP (fAHP) and medium AHP (mAHP) after OT
545 application respective to baseline (pre). The amplitudes of the fAHP and mAHP following the
546 first action potential evoked at Rh were calculated as the difference from the action potential
547 threshold to the membrane voltage measured after 2-5 msec and 50-100 msec, respectively.
548 The IAHP was measured at 2000 msec after the end of the depolarizing pulse, following
549 generation of five action potentials. **B**: Line graphs showing individual neurons' responses (gray)
550 and reduction of the fAHP during OT application (*P* = 0.0124, F (1.473, 17.68 = 6.493, mixed-
551 effects analysis, n = 14). **C**: OTR antagonist, OTA (0.4 μM), prevents the OT-induced reduction
552 of fAHP (*P* = 0.2220, n = 7, RM one-way ANOVA). **D**: Line graph showing reduction of mAHP
553 during OT application (*P* <0.0001, F (1.844, 22.13) = 23.25, mixed effect analysis, n = 14). **E***:*
554 OT-induced reduction of mAHP is blocked by OTR antagonist, OTA (*P* = 0.3968, n = 7, RM one-
555 way ANOVA). Thick black lines show average responses for all Type I neurons recorded. **F**: OT
556 modifies early and late spike frequency adaptation. The early and late spike frequency
557 adaptation was investigated using a depolarizing pulse of 1 sec and measuring the
558 instantaneous frequency for every action potential interval. The ISI number is the inter-stimulus
559 interval between two consecutive action potentials. OT significantly increased the instantaneous
560 frequency of ISI (*P* < 0.0001, F (1, 13) = 82.69, mixed effects model). Each data point
561 represents the mean ± SEM, ****P* < 0.0001, ***P* < 0.001, **P* < 0.01, **P* < 0.05.

562 **Figure 4. Oxytocin increases spontaneous firing rate of Type I neurons and reduces**
563 **spontaneous firing rate of Type II $BNST_{DL}$ neurons in cell-attached recordings**. **A**: A
564 representative trace of Type I neuron showing an increase in spontaneous firing rate after OT
565 application. **B**: Line graph showing that OT increased spontaneous firing rate in all
566 spontaneously firing Type I neurons (P = 0.0242, paired t-test, n = 7), gray lines represent
567 individual neurons' responses, thick black line represents average response. **C**: A
568 representative trace of Type II neuron showing a reduction in spontaneous firing rate after OT
569 application. **D**: Line graph showing that OT reduced spontaneous firing rate in spontaneously
570 firing Type II neurons in cell-attached mode (P = 0.0525, paired t-test, n = 6).

571 **Figure 5. Oxytocin modulates inhibitory synaptic transmission in $BNST_{DL}$ neurons. A**:
572 Representative recordings showing an increase in the frequency of spontaneous inhibitory
573 postsynaptic currents (sIPSCs) after OT application respective to baseline (pre). **B-C**: Line
574 graphs (gray) showing that 12 out of 14 recorded Type II neurons showed an increase in
575 sIPSCs frequency (**B**, P = 0.0022, F (1.058, 12.17) = 14.41, n = 14, mixed-effect analysis) but
576 not amplitude (**C**, P = 0.5855, F (1.563, 17.19) = 0.4718, n = 14, mixed-effect analysis) after OT
577 application. **D**: OT does not affect sIPSC frequency in a presence of OTR antagonist, OTA (0.4
578 μM) (P = 0.1788, F (1.469, 8.814) = 2.135, n = 6, RM ANOVA). **E**: When spike-driven IPSCs
579 were blocked with TTX (P = 0.0151, F (1.030, 6.179) = 10.98, n = 6, RM ANOVA), OT does not
580 affect the sIPSCs frequency. **F-G**: OT does not affect frequency (**F**, P = 0.9362) but reduces
581 amplitude of sIPCS in Type III neurons (**G**, P = 0.0160, paired t-test). Thick black lines show
582 averaged responses for all neurons recorded. Each data point represents the mean ± SEM, **P
583 < 0.01, *P < 0.05 in comparison to pre- or post-OT.

584 **Figure 6. Oxytocin increases amplitude of evoked IPSCs in Type III, but not Type II**
585 **neurons**. **A:** Representative traces of eIPSC in response to the electrical stimulation of the stria
586 terminalis in Type II neurons. **B**: Line graph showing that OT does not significantly change the
587 mean amplitude of eIPSC in Type II neurons (P = 0.2459, paired t-test). Thick black lines show

588 averaged responses for all neurons recorded. **C:** Representative traces of eIPSCs in Type III
589 neurons showing reduction of the eIPSCs amplitude after OT application. **D-E:** Line graphs
590 showing individual Type III neurons and the reduction of the eIPSC amplitude after OT (**D**, P =
591 0.0105) without any significant change in the PPR (**E**, P = 0.5672).

592 **Figure 7. Type II neurons are output neurons of the $BNST_{DL}$ to the central amygdala. A-B**:
593 Microphotographs showing neurons expressing green fluorescent microbeads in the $BNST_{DL}$
594 after the retrobeads were injected into the central amygdala (CeA). **A**: BNST neurons projecting
595 to the CeA (*BNST➔CeA* neurons) were primarily found in the dorsolateral BNST, primarily the
596 oval nucleus, and to a lesser extent in the anteromedial BNST (20x, LV – Lateral ventricle, IC –
597 Internal capsulae, $BNST_{AM}$ - anteriomedial BNST, $BNST_{OV}$ - oval nucleus of the BNST, scale
598 bar 100 μm). **B**: High magnification (60x) microphotographs showing green fluorescent beads
599 present in membranes and processes of the *BNST➔CeA* neurons (scale bar 10 μm). **C-D**:
600 Electrophysiological characterization of the *BNST➔CeA* neurons using visually guided patching
601 (**C**, 40x, scale bar 20 μm). Representative recording of the BNST➔CeA fluorescent neuron
602 showing the electrophysiological properties of a Type II neuron such as the presence of a sag
603 during the hyperpolarized current pulses and the spike rebound at the end of the 450 ms current
604 pulse injection (**D**). **E**: Diagram showing that OT regulates the intrinsic inhibitory network and
605 inhibits output neurons of the $BNST_{DL}$. By directly increasing frequency of spontaneous firing of
606 Type I regular spiking neurons, OT inhibits firing of Type II $BNST_{DL}$ neurons. Type II neurons
607 are output neurons of the $BNST_{DL}$ sending projections to the central amygdala (*BNST➔CeA*
608 neurons*)*. OT also inhibits another class of output neurons, Type III, via a direct postsynaptic
609 mechanism. Therefore, OT excites $BNST_{DL}$ interneurons (Type I) and inhibits two classes of the
610 $BNST_{DL}$ projection neurons via distinct indirect (Type II) and direct (Type III) mechanisms,
611 respectively.

612 **9. References**

613 al-Shamma HA, De Vries GJ. 1996. Neurogenesis of the sexually dimorphic vasopressin cells of
614 the bed nucleus of the stria terminalis and amygdala of rats. *J Neurobiol* **29**:91–98.
615 doi:10.1002/(SICI)1097-4695(199601)29:1<91::AID-NEU7>3.0.CO;2-2
616 Alger BE, Nicoll RA. 1980. Epileptiform burst afterhyperolarization: calcium-dependent
617 potassium potential in hippocampal CA1 pyramidal cells. *Science* **210**:1122–1124.
618 doi:10.1126/science.7444438
619 Alheid GF. 2003. Extended amygdala and basal forebrain. *Ann N Y Acad Sci* **985**:185–205.
620 Beyeler A, Dabrowska J. 2020. Neuronal diversity of the amygdala and the bed nucleus of the
621 stria terminalis. *Handb Behav Neurosci* **26**:63–100. doi:10.1016/b978-0-12-815134-
622 1.00003-9
623 Bosch OJ, Young LJ. 2018. Oxytocin and Social Relationships: From Attachment to Bond
624 Disruption. *Curr Top Behav Neurosci* **35**:97–117. doi:10.1007/7854_2017_10
625 Brussaard AB, Kits KS, de Vlieger TA. 1996. Postsynaptic mechanism of depression of
626 GABAergic synapses by oxytocin in the supraoptic nucleus of immature rat. *J Physiol*
627 **497 (Pt 2)**:495–507. doi:10.1113/jphysiol.1996.sp021783
628 Caldeyro-Barcia R, Poseiro JJ. 1959. Oxytocin and contractility of the pregnant human uterus.
629 *Ann N Y Acad Sci* **75**:813–830.
630 Crane JW, Holmes NM, Fam J, Westbrook RF, Delaney AJ. 2020. Oxytocin increases inhibitory
631 synaptic transmission and blocks development of long-term potentiation in the lateral
632 amygdala. *J Neurophysiol* **123**:587–599. doi:10.1152/jn.00571.2019
633 Cullinan WE, Herman JP, Watson SJ. 1993. Ventral subicular interaction with the hypothalamic
634 paraventricular nucleus: evidence for a relay in the bed nucleus of the stria terminalis. *J*
635 *Comp Neurol* **332**:1–20. doi:10.1002/cne.903320102
636 Dabrowska J, Hazra R, Ahern TH, Guo J-D, McDonald AJ, Mascagni F, Muller JF, Young LJ,
637 Rainnie DG. 2011. Neuroanatomical evidence for reciprocal regulation of the
638 corticotrophin-releasing factor and oxytocin systems in the hypothalamus and the bed

639 nucleus of the stria terminalis of the rat: Implications for balancing stress and affect.
640 *Psychoneuroendocrinology* **36**:1312–1326. doi:10.1016/j.psyneuen.2011.03.003
641 Dabrowska J, Hazra R, Guo J-D, Dewitt S, Rainnie DG. 2013a. Central CRF neurons are not
642 created equal: phenotypic differences in CRF-containing neurons of the rat
643 paraventricular hypothalamus and the bed nucleus of the stria terminalis. *Front Neurosci*
644 **7**:156. doi:10.3389/fnins.2013.00156
645 Dabrowska J, Hazra R, Guo J-D, Li C, Dewitt S, Xu J, Lombroso PJ, Rainnie DG. 2013b.
646 Striatal-enriched protein tyrosine phosphatase-STEPs toward understanding chronic
647 stress-induced activation of corticotrophin releasing factor neurons in the rat bed nucleus
648 of the stria terminalis. *Biol Psychiatry* **74**:817–826. doi:10.1016/j.biopsych.2013.07.032
649 Dabrowska J, Martinon D, Moaddab M, Rainnie DG. 2016. Targeting Corticotropin-Releasing
650 Factor Projections from the Oval Nucleus of the Bed Nucleus of the Stria Terminalis
651 Using Cell-Type Specific Neuronal Tracing Studies in Mouse and Rat Brain. *J*
652 *Neuroendocrinol* **28**. doi:10.1111/jne.12442
653 Daniel SE, Guo J, Rainnie DG. 2017. A comparative analysis of the physiological properties of
654 neurons in the anterolateral bed nucleus of the stria terminalis in the Mus musculus,
655 Rattus norvegicus, and Macaca mulatta. *J Comp Neurol* **525**:2235–2248.
656 doi:10.1002/cne.24202
657 Daniel SE, Rainnie DG. 2016. Stress Modulation of Opposing Circuits in the Bed Nucleus of the
658 Stria Terminalis. *Neuropsychopharmacology* **41**:103–125. doi:10.1038/npp.2015.178
659 Davis M, Walker DL, Miles L, Grillon C. 2010. Phasic vs sustained fear in rats and humans: role
660 of the extended amygdala in fear vs anxiety. *Neuropsychopharmacology* **35**:105–135.
661 doi:10.1038/npp.2009.109
662 Dumais KM, Bredewold R, Mayer TE, Veenema AH. 2013. Sex differences in oxytocin receptor
663 binding in forebrain regions: correlations with social interest in brain region- and sex-
664 specific ways. *Horm Behav* **64**:693–701. doi:10.1016/j.yhbeh.2013.08.012

665 Duvarci S, Bauer EP, Paré D. 2009. The bed nucleus of the stria terminalis mediates inter-
666 individual variations in anxiety and fear. *J Neurosci* **29**:10357–10361.
667 doi:10.1523/JNEUROSCI.2119-09.2009
668 Eliava M, Melchior M, Knobloch-Bollmann HS, Wahis J, da Silva Gouveia M, Tang Y, Ciobanu
669 AC, Triana Del Rio R, Roth LC, Althammer F, Chavant V, Goumon Y, Gruber T, Petit-
670 Demoulière N, Busnelli M, Chini B, Tan LL, Mitre M, Froemke RC, Chao MV, Giese G,
671 Sprengel R, Kuner R, Poisbeau P, Seeburg PH, Stoop R, Charlet A, Grinevich V. 2016.
672 A New Population of Parvocellular Oxytocin Neurons Controlling Magnocellular Neuron
673 Activity and Inflammatory Pain Processing. *Neuron* **89**:1291–1304.
674 doi:10.1016/j.neuron.2016.01.041
675 Francesconi W, Berton F, Repunte-Canonigo V, Hagihara K, Thurbon D, Lekic D, Specio SE,
676 Greenwell TN, Chen SA, Rice KC, Richardson HN, O'Dell LE, Zorrilla EP, Morales M,
677 Koob GF, Sanna PP. 2009. Protracted withdrawal from alcohol and drugs of abuse
678 impairs long-term potentiation of intrinsic excitability in the juxtacapsular bed nucleus of
679 the stria terminalis. *J Neurosci* **29**:5389–5401. doi:10.1523/JNEUROSCI.5129-08.2009
680 Goode TD, Acca GM, Maren S. 2020. Threat imminence dictates the role of the bed nucleus of
681 the stria terminalis in contextual fear. *Neurobiol Learn Mem* **167**:107116.
682 doi:10.1016/j.nlm.2019.107116
683 Goode TD, Ressler RL, Acca GM, Miles OW, Maren S. 2019. Bed nucleus of the stria terminalis
684 regulates fear to unpredictable threat signals. *Elife* **8**. doi:10.7554/eLife.46525
685 Gozzi A, Jain A, Giovannelli A, Giovanelli A, Bertollini C, Crestan V, Schwarz AJ, Tsetsenis T,
686 Ragozzino D, Gross CT, Bifone A. 2010. A neural switch for active and passive fear.
687 *Neuron* **67**:656–666. doi:10.1016/j.neuron.2010.07.008
688 Grundwald NJ, Benítez DP, Brunton PJ. 2016. Sex-Dependent Effects of Prenatal Stress on
689 Social Memory in Rats: A Role for Differential Expression of Central Vasopressin-1a
690 Receptors. *J Neuroendocrinol* **28**. doi:10.1111/jne.12343

691 Gu N, Hu H, Vervaeke K, Storm JF. 2008. SK (KCa2) channels do not control somatic
692 excitability in CA1 pyramidal neurons but can be activated by dendritic excitatory
693 synapses and regulate their impact. *J Neurophysiol* **100**:2589–2604.
694 doi:10.1152/jn.90433.2008
695 Gu N, Vervaeke K, Hu H, Storm JF. 2005a. Kv7/KCNQ/M and HCN/h, but not KCa2/SK
696 channels, contribute to the somatic medium after-hyperpolarization and excitability
697 control in CA1 hippocampal pyramidal cells. *J Physiol (Lond)* **566**:689–715.
698 doi:10.1113/jphysiol.2005.086835
699 Gu N, Vervaeke K, Hu H, Storm JF. 2005b. Kv7/KCNQ/M and HCN/h, but not KCa2/SK
700 channels, contribute to the somatic medium after-hyperpolarization and excitability
701 control in CA1 hippocampal pyramidal cells. *J Physiol (Lond)* **566**:689–715.
702 doi:10.1113/jphysiol.2005.086835
703 Gu N, Vervaeke K, Storm JF. 2007. BK potassium channels facilitate high-frequency firing and
704 cause early spike frequency adaptation in rat CA1 hippocampal pyramidal cells. *J*
705 *Physiol (Lond)* **580**:859–882. doi:10.1113/jphysiol.2006.126367
706 Gungor NZ, Paré D. 2016. Functional Heterogeneity in the Bed Nucleus of the Stria Terminalis.
707 *J Neurosci* **36**:8038–8049. doi:10.1523/JNEUROSCI.0856-16.2016
708 Gungor NZ, Yamamoto R, Paré D. 2015. Optogenetic study of the projections from the bed
709 nucleus of the stria terminalis to the central amygdala. *J Neurophysiol* **114**:2903–2911.
710 doi:10.1152/jn.00677.2015
711 Hammack SE, Mania I, Rainnie DG. 2007. Differential expression of intrinsic membrane
712 currents in defined cell types of the anterolateral bed nucleus of the stria terminalis. *J*
713 *Neurophysiol* **98**:638–656. doi:10.1152/jn.00382.2007
714 Han JS, Maeda Y, Knepper MA. 1993. Dual actions of vasopressin and oxytocin in regulation of
715 water permeability in terminal collecting duct. *Am J Physiol* **265**:F26-34.
716 doi:10.1152/ajprenal.1993.265.1.F26

717 Harden SW, Frazier CJ. 2016. Oxytocin depolarizes fast-spiking hilar interneurons and induces
718 GABA release onto mossy cells of the rat dentate gyrus. *Hippocampus* **26**:1124–1139.
719 doi:10.1002/hipo.22595
720 Huber D, Veinante P, Stoop R. 2005. Vasopressin and oxytocin excite distinct neuronal
721 populations in the central amygdala. *Science* **308**:245–248.
722 doi:10.1126/science.1105636
723 Hung LW, Neuner S, Polepalli JS, Beier KT, Wright M, Walsh JJ, Lewis EM, Luo L, Deisseroth
724 K, Dölen G, Malenka RC. 2017. Gating of social reward by oxytocin in the ventral
725 tegmental area. *Science* **357**:1406–1411. doi:10.1126/science.aan4994
726 Ingram CD, Cutler KL, Wakerley JB. 1990. Oxytocin excites neurones in the bed nucleus of the
727 stria terminalis of the lactating rat in vitro. *Brain Res* **527**:167–170.
728 Ingram CD, Moos F. 1992. Oxytocin-containing pathway to the bed nuclei of the stria terminalis
729 of the lactating rat brain: immunocytochemical and in vitro electrophysiological evidence.
730 *Neuroscience* **47**:439–452.
731 Janeček M, Dabrowska J. 2019. Oxytocin facilitates adaptive fear and attenuates anxiety
732 responses in animal models and human studies-potential interaction with the
733 corticotropin-releasing factor (CRF) system in the bed nucleus of the stria terminalis
734 (BNST). *Cell Tissue Res* **375**:143–172. doi:10.1007/s00441-018-2889-8
735 Knobloch HS, Charlet A, Hoffmann LC, Eliava M, Khrulev S, Cetin AH, Osten P, Schwarz MK,
736 Seeburg PH, Stoop R, Grinevich V. 2012. Evoked axonal oxytocin release in the central
737 amygdala attenuates fear response. *Neuron* **73**:553–566.
738 doi:10.1016/j.neuron.2011.11.030
739 Kremarik P, Freund-Mercier MJ, Stoeckel ME. 1991. Autoradiographic detection of oxytocin-
740 and vasopressin-binding sites in various subnuclei of the bed nucleus of the stria
741 terminalis in the rat. Effects of functional and experimental sexual steroid variations. *J*
742 *Neuroendocrinol* **3**:689–698. doi:10.1111/j.1365-2826.1991.tb00335.x

743 Lopez de Armentia M, Sah P. 2004. Firing properties and connectivity of neurons in the rat
744 lateral central nucleus of the amygdala. *J Neurophysiol* **92**:1285–1294.
745 doi:10.1152/jn.00211.2004
746 Maejima S, Ohishi N, Yamaguchi S, Tsukahara S. 2015. A neural connection between the
747 central part of the medial preoptic nucleus and the bed nucleus of the stria terminalis to
748 regulate sexual behavior in male rats. *Neurosci Lett* **606**:66–71.
749 doi:10.1016/j.neulet.2015.08.047
750 Maniezzi C, Talpo F, Spaiardi P, Toselli M, Biella G. 2019. Oxytocin Increases Phasic and Tonic
751 GABAergic Transmission in CA1 Region of Mouse Hippocampus. *Front Cell Neurosci*
752 **13**:178. doi:10.3389/fncel.2019.00178
753 Manning M, Misicka A, Olma A, Bankowski K, Stoev S, Chini B, Durroux T, Mouillac B, Corbani
754 M, Guillon G. 2012. Oxytocin and vasopressin agonists and antagonists as research
755 tools and potential therapeutics. *J Neuroendocrinol* **24**:609–628. doi:10.1111/j.1365-
756 2826.2012.02303.x
757 Marlin BJ, Mitre M, D'amour JA, Chao MV, Froemke RC. 2015. Oxytocin enables maternal
758 behaviour by balancing cortical inhibition. *Nature* **520**:499–504.
759 doi:10.1038/nature14402
760 Martina M, Kilić G, Cherubini E. 1994. The effect of intracellular Ca2+ on GABA-activated
761 currents in cerebellar granule cells in culture. *J Membr Biol* **142**:209–216.
762 doi:10.1007/BF00234942
763 Martinon D, Lis P, Roman AN, Tornesi P, Applebey SV, Buechner G, Olivera V, Dabrowska J.
764 2019. Oxytocin receptors in the dorsolateral bed nucleus of the stria terminalis (BNST)
765 bias fear learning toward temporally predictable cued fear. *Transl Psychiatry* **9**:140.
766 doi:10.1038/s41398-019-0474-x
767 McDonald AJ, Shammah-Lagnado SJ, Shi C, Davis M. 1999. Cortical afferents to the extended
768 amygdala. *Ann N Y Acad Sci* **877**:309–338.

769 Meloni EG, Jackson A, Gerety LP, Cohen BM, Carlezon WA. 2006. Role of the bed nucleus of
770 the stria terminalis (BST) in the expression of conditioned fear. *Ann N Y Acad Sci*
771 **1071**:538–541. doi:10.1196/annals.1364.059
772 Moaddab M, Dabrowska J. 2017. Oxytocin receptor neurotransmission in the dorsolateral bed
773 nucleus of the stria terminalis facilitates the acquisition of cued fear in the fear-
774 potentiated startle paradigm in rats. *Neuropharmacology* **121**:130–139.
775 doi:10.1016/j.neuropharm.2017.04.039
776 Nakajima M, Görlich A, Heintz N. 2014. Oxytocin modulates female sociosexual behavior
777 through a specific class of prefrontal cortical interneurons. *Cell* **159**:295–305.
778 doi:10.1016/j.cell.2014.09.020
779 Neumann ID, Slattery DA. 2016. Oxytocin in General Anxiety and Social Fear: A Translational
780 Approach. *Biol Psychiatry* **79**:213–221. doi:10.1016/j.biopsych.2015.06.004
781 Nickerson K, Bonsness RW, Douglas RG, Condliffe P, Du Vigneaud V. 1954. Oxytocin and milk
782 ejection. *Am J Obstet Gynecol* **67**:1028–1034.
783 Okamura H, Abitbol M, Julien JF, Dumas S, Bérod A, Geffard M, Kitahama K, Bobillier P, Mallet
784 J, Wiklund L. 1990. Neurons containing messenger RNA encoding glutamate
785 decarboxylase in rat hypothalamus demonstrated by in situ hybridization, with special
786 emphasis on cell groups in medial preoptic area, anterior hypothalamic area and
787 dorsomedial hypothalamic nucleus. *Neuroscience* **39**:675–699. doi:10.1016/0306-
788 4522(90)90252-y
789 Olivera-Pasilio V, Dabrowska J. 2020. Oxytocin Promotes Accurate Fear Discrimination and
790 Adaptive Defensive Behaviors. *Front Neurosci* **14**:583878.
791 doi:10.3389/fnins.2020.583878
792 Owen SF, Tuncdemir SN, Bader PL, Tirko NN, Fishell G, Tsien RW. 2013. Oxytocin enhances
793 hippocampal spike transmission by modulating fast-spiking interneurons. *Nature*
794 **500**:458–462. doi:10.1038/nature12330

795 Pedarzani P, Storm JF. 1993. PKA mediates the effects of monoamine transmitters on the K+
796 current underlying the slow spike frequency adaptation in hippocampal neurons. *Neuron*
797 **11**:1023–1035. doi:10.1016/0896-6273(93)90216-e
798 Pedersen CA, Caldwell JD, Peterson G, Walker CH, Mason GA. 1992. Oxytocin activation of
799 maternal behavior in the rat. *Ann N Y Acad Sci* **652**:58–69.
800 Perkins KL. 2006. Cell-attached voltage-clamp and current-clamp recording and stimulation
801 techniques in brain slices. *J Neurosci Methods* **154**:1–18.
802 doi:10.1016/j.jneumeth.2006.02.010
803 Rodríguez-Sierra OE, Turesson HK, Pare D. 2013. Contrasting distribution of physiological cell
804 types in different regions of the bed nucleus of the stria terminalis. *J Neurophysiol*
805 **110**:2037–2049. doi:10.1152/jn.00408.2013
806 Sharma K, LeBlanc R, Haque M, Nishimori K, Reid MM, Teruyama R. 2019. Sexually dimorphic
807 oxytocin receptor-expressing neurons in the preoptic area of the mouse brain. *PLoS*
808 *ONE* **14**:e0219784. doi:10.1371/journal.pone.0219784
809 Simerly RB, Swanson LW. 1988. Projections of the medial preoptic nucleus: a Phaseolus
810 vulgaris leucoagglutinin anterograde tract-tracing study in the rat. *J Comp Neurol*
811 **270**:209–242. doi:10.1002/cne.902700205
812 Sparta DR, Jennings JH, Ung RL, Stuber GD. 2013. Optogenetic strategies to investigate neural
813 circuitry engaged by stress. *Behav Brain Res* **255**:19–25. doi:10.1016/j.bbr.2013.05.007
814 Sullivan GM, Apergis J, Bush DEA, Johnson LR, Hou M, Ledoux JE. 2004. Lesions in the bed
815 nucleus of the stria terminalis disrupt corticosterone and freezing responses elicited by a
816 contextual but not by a specific cue-conditioned fear stimulus. *Neuroscience* **128**:7–14.
817 doi:10.1016/j.neuroscience.2004.06.015
818 Sun N, Cassell MD. 1993. Intrinsic GABAergic neurons in the rat central extended amygdala. *J*
819 *Comp Neurol* **330**:381–404. doi:10.1002/cne.903300308
820 Tabbaa M, Paedae B, Liu Y, Wang Z. 2016. Neuropeptide Regulation of Social Attachment: The
821 Prairie Vole Model. *Compr Physiol* **7**:81–104. doi:10.1002/cphy.c150055

822 Terburg D, Scheggia D, Triana Del Rio R, Klumpers F, Ciobanu AC, Morgan B, Montoya ER,
823 Bos PA, Giobellina G, van den Burg EH, de Gelder B, Stein DJ, Stoop R, van Honk J.
824 2018. The Basolateral Amygdala Is Essential for Rapid Escape: A Human and Rodent
825 Study. *Cell* **175**:723-735.e16. doi:10.1016/j.cell.2018.09.028
826 Tirko NN, Eyring KW, Carcea I, Mitre M, Chao MV, Froemke RC, Tsien RW. 2018. Oxytocin
827 Transforms Firing Mode of CA2 Hippocampal Neurons. *Neuron* **100**:593-608.e3.
828 doi:10.1016/j.neuron.2018.09.008
829 Tribollet E, Dubois-Dauphin M, Dreifuss JJ, Barberis C, Jard S. 1992. Oxytocin receptors in the
830 central nervous system. Distribution, development, and species differences. *Ann N Y*
831 *Acad Sci* **652**:29–38.
832 Veinante P, Freund-Mercier MJ. 1997. Distribution of oxytocin- and vasopressin-binding sites in
833 the rat extended amygdala: a histoautoradiographic study. *J Comp Neurol* **383**:305–325.
834 Verbalis JG, Blackburn RE, Olson BR, Stricker EM. 1993. Central oxytocin inhibition of food and
835 salt ingestion: a mechanism for intake regulation of solute homeostasis. *Regul Pept*
836 **45**:149–154.
837 Viviani D, Charlet A, van den Burg E, Robinet C, Hurni N, Abatis M, Magara F, Stoop R. 2011.
838 Oxytocin selectively gates fear responses through distinct outputs from the central
839 amygdala. *Science* **333**:104–107. doi:10.1126/science.1201043
840 Waddell J, Morris RW, Bouton ME. 2006. Effects of bed nucleus of the stria terminalis lesions
841 on conditioned anxiety: aversive conditioning with long-duration conditional stimuli and
842 reinstatement of extinguished fear. *Behav Neurosci* **120**:324–336. doi:10.1037/0735-
843 7044.120.2.324
844 Wilson BC, Terenzi MG, Ingram CD. 2005. Differential excitatory responses to oxytocin in sub-
845 divisions of the bed nuclei of the stria terminalis. *Neuropeptides* **39**:403–407.
846 doi:10.1016/j.npep.2005.04.001

847 Xiao L, Priest MF, Nasenbeny J, Lu T, Kozorovitskiy Y. 2017. Biased Oxytocinergic Modulation
848 of Midbrain Dopamine Systems. *Neuron* **95**:368-384.e5.
849 doi:10.1016/j.neuron.2017.06.003
850 Xu X, Ikrar T, Sun Y, Santos R, Holmes TC, Francesconi W, Berton F. 2016. High-resolution
851 and cell-type-specific photostimulation mapping shows weak excitatory vs. strong
852 inhibitory inputs in the bed nucleus of the stria terminalis. *J Neurophysiol* **115**:3204–
853 3216. doi:10.1152/jn.01148.2015
854 Zaninetti M, Raggenbass M. 2000. Oxytocin receptor agonists enhance inhibitory synaptic
855 transmission in the rat hippocampus by activating interneurons in stratum pyramidale.
856 *Eur J Neurosci* **12**:3975–3984. doi:10.1046/j.1460-9568.2000.00290.x
857